EVAPOTRANSPIRATION IN DRY CLIMATE AREA: COMPARING REMOTE SENSING TECHNIQUES WITH UNSATURATED ZONE WATER FLOW SIMULATION

IDHAM EFFENDI
February, 2012

SUPERVISORS:
Dr. Ir. Christiaan van der Tol
Dr. Ir. M.W. Lubczynski

ADVISOR:
MSc. Enrico Balugani (PhD Candidate)

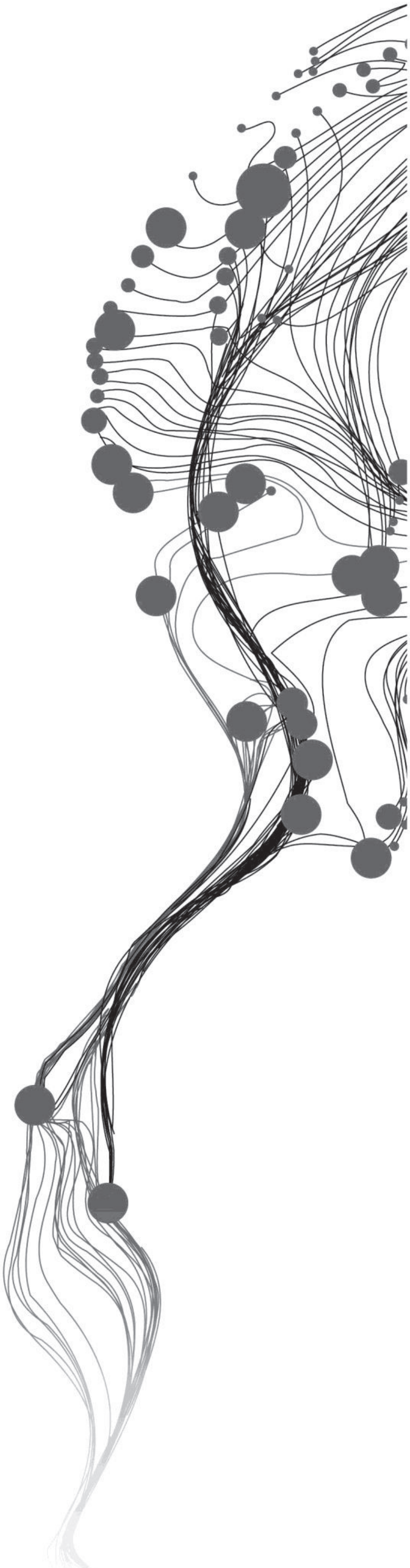

EVAPOTRANSPIRATION IN DRY CLIMATE AREA: COMPARING REMOTE SENSING TECHNIQUES WITH UNSATURATED ZONE WATER FLOW SIMULATION

IDHAM EFFENDI

Enschede, The Netherlands, February 2012

Thesis submitted to the Faculty of Geo-Information Science and Earth Observation of the University of Twente in partial fulfilment of the requirements for the degree of Master of Science in Geo-information Science and Earth Observation.
Specialization: Water Resources and Environmental Management

SUPERVISORS:
Dr. Ir. Christiaan van der Tol
Dr. Ir. M.W. Lubczynski

THESIS ASSESSMENT BOARD:
Prof. Dr. Z. Su (Chairman)
Prof. Dr. O. Batelaan (External Examiner, Vrije Universiteit Brussel)

ABSTRACT

An overestimation of evapotranspiration obtained by remote sensing approach has been found in earlier studies in Sardon. This problem is more general: it occurs in similar areas characterized by water limited environment and sparse vegetation area too. This study is aimed to compare the ability of two different approaches; notably a remote sensing (RS) approach and a hydrological model simulation approach, to estimate evapotranspiration in dry climate area. The selected study area is located in Sardon, near Salamanca, a region in the west of Spain which represents a typical semi-arid land area. The study focused on dry season in 2009 and 2010.

In RS approach, two different methods were applied, namely SEBS and Simple Energy Balance. As satellite images input, two LANDSAT 5 TM images of 2009 and two of 2010 were used. HYDRUS 1D was chosen as hydrological model to simulate the soil evaporation in the area. By assigning input parameter in pre-processing, like geometry information, soil hydraulic parameter and boundary conditions, HYDRUS 1D model was simulated to produce actual surface fluxes, including evaporation flux (E). By integrating that E with transpiration (T), AET was obtained. Eddy covariance (EC) is one method of direct measurement approaches which has been widely applied in calculating evapotranspiration. Evapotranspiration of eddy covariance was calculated from the contribution of the related footprint area. This method is used as reference for validation of ET estimation methods.

The results shown that in 2009 AET estimated with the RS approach is higher than AET estimated with HYDRUS 1D. The average AET value in 17 RS pixels corresponding to the HYDRUS 1D points at the time of the satellite overpass are 0.632, 0.667, and 0.392 $mm.d^{-1}$ for the SEBS, the simple energy balance and HYDRUS 1D, respectively. In 2010, due to high wind speed during this period, the AET value of SEBS is much lower than the simple energy balance. Therefore, the average AET values of each method are 0.156, 0.995, and 0.218 $mm.d^{-1}$ for the SEBS, the simple energy balance and HYDRUS 1D, respectively. However, spatially AET values of RS and HYDRUS 1D did not correlate well.

HYDRUS 1D as the chosen hydrological modelling shows a better agreement to the EC method than the RS approach. The output of HYDRUS 1D model is a time series of AET values; this permits the comparison with the time series data of AET measured by EC. On the other hand, with the RS approach is possible to obtain the spatial distribution of AET, which can be compared with EC measurements calculating the related footprint area.

The integration of both approaches; RS approach and hydrological modelling approach, is required to understand better how ET varies, both in space and time, in semi arid areas.

Key words: evapotranspiration, remote sensing, SEBS, HYDRUS 1D, eddy covariance

ACKNOWLEDGEMENTS

Alhamdulillah, praise to be Allah, The All-Knowing and The All-Powerful; for providing me the opportunity to step in the excellent world of science. Nothing I have achieved is without His Will, Guidance and Permission.

I would like to extend my sincere appreciation to some very special people and community, who have contributed with their knowledge, time, and support in completing this thesis.

Dr. Ir. Christiaan van der Tol, my first supervisor, comes first in this row, who have opened himself up to me with his enormous knowledge and guided me continuously throughout the completion of this work. Likewise, I am thankful to Dr. Ir. Maciek W. Lubczynski, my second supervisor, for being supportive and providing valuable comments. I believe his valuable suggestion and criticism have enhanced the quality of the work. I would like to thank to my advisor, Enrico Balugani for his valuable remarks and reviews to the work.

I also want to express my gratitude to the research group in the Sardon catchment, thanks for all the comments and assistance during this period. I extend my gratitude to Dr. Boudewijn de Smeth for his guidance throughout laboratory stage.

Many thanks for my terrific Indonesian friends in PPI Enschede, for providing environment of home feeling. Special acknowledgement goes to Arie Yulfa, Fitriani Agustin, Rani Charisma Dewi, Hidayah Hamzah, Nugroho Christanto, Doddy M. Yuwono, Fesly Paranoan, Debi Mutia, Tiur Hotdelima, Kang Syarif Budhiman, Pakde Winardi, Pak Anas Fauzi, for sharing their companionship and good times together.

I would like to thank to all WREM (2010-2012) classmates from all around the world, for their friendship and encouragement. My acknowledgement goes particularly to Tikaram Baral, Etefa Rundassa Daba, and Ugyen Eden, were helpful in the brainstorming sessions during the thesis period.

Last but not the least, my deepest gratitude goes to my family for their unflagging love and support throughout my life; this thesis is simply impossible without them.

Idham Effendi

February 2012, Enschede - the Netherlands.

TABLE OF CONTENTS

LIST OF FIGURES

LIST OF TABLES

1. INTRODUCTION

1.1. Background

Evapotranspiration is the second most component of the hydrologic cycle, after precipitation (Brutsaert, 2005). Together with rainfall and runoff, evapotranspiration controls the availability of water at the Earth surface. Estimation of evapotranspiration as a component of hydrologic cycle is needed in wide range of a lot of problems in hydrology, forestry and water resources planning. Evapotranspiration is the physical phenomenon of conversion of liquid phase to the vapour phase (Brutsaert, 2005). Evapotranspiration appears in both water balance equation and land surface energy balance. Amongst the water balance components, evapotranspiration from land surface and vegetation is often the most difficult to estimate. Therefore, accurate estimation of evapotranspiration is imperative in managing water resources, especially in arid or semi-arid areas.

Land-based data, satellite data, and computer models are different methods for giving explanation about the complex time and space variations of physical processes produced by the climate system and the hydrologic cycle (Shelton, 2008). There is well developed research about the methods for the estimation of evapotranspiration. Each method offer different approach, which also requires different parameters.

In recent of years, many studies have tried to estimate evapotranspiration using remote sensing approach. Remote sensing approach has numerous advantages for evaluating hydrometeorological variables including evapotranspiration over large area (Kite & Pietroniro, 1996). Remote sensing data is also now widely available and easily accessible which then can be used for any purposes. In estimating evapotranspiration, remote sensing technique is important to resolve the challenge of the spatial distribution in large area, although the continuous time series analyses are difficult. The main advantage of remote sensing approach is that evapotranspiration on a large scale can be calculated by utilizing the spectral radiance value of each pixel of satellite image. Even with limited ground measurements are available, remotely sensed evapotranspiration can both express model structural deficiencies and condition model parameters (Winsemius et al., 2008).

By simulation of a certain hydrological model, evapotranspiration of the research area will be estimated based on ground measurement data. A number of hydrological models were developed in the past to solve the water balance for given areas. These models varies in complexity going from simple analytical models to complex systems of differential equation solved with numerical model implemented in computer programs (Schuurmans et al., 2003). However, hydrologic models have some limitations. The major problems are over-parameterization and uncertainty, most models have not been validated due to the lack of appropriate of datasets (Schaap et al., 2001).

This study focuses on Sardon catchment, which is located in the central-western part of Iberian Peninsula with typically semi-arid climate area with an average yearly precipitation ≈ 500 mm/yr (Lubczynski & Gurwin, 2005). Some studies had been performed numerously in the study area, concerning specific interests, such as geology, hydrology and hydrogeology. Worku (2000) performed remote sensing approach for estimating evapotranspiration in Sardon catchment. He applied SEBAL algorithm in different dates of dry season; June 23, 1999 and September 11, 1999. The results of the estimated actual evapotranspiration were 0 – 6 $mm.d^{-1}$ in June and 0 - 4.3 $mm.d^{-1}$ in September. By applying this value of actual evapotranspiration in numerical groundwater MODFLOW model, these results are unlikely when balancing all the fluxes in the catchment (Lubczynski & Gurwin, 2005).

Therefore, integrating the capabilities of hydrological model simulation and remote sensing techniques is imperative for our knowledge in hydrological processes and also important related to the matter of water resource management. Winsemius, et al (2008) explained a method of remotely sensed evapotranspiration which can be applied to construct distributions of land-surface related parameter in hydrological models. Hopefully, the combination of these two approaches, remote sensing and hydrological modelling for the estimation of evapotranspiration can give a better understanding about how the availability of evapotranspiration varies both spatially and temporally.

1.2. Problem definition

The problem of this study is that the value of actual evapotranspiration which is important as input for applying groundwater model (e.g. MODFLOW) is not well known, spatially and temporally, in the Sardon catchment area. Two approaches which use a different technique in estimating actual evapotranspiration, namely remote sensing approach and hydrological model simulation approach, should be carried out to obtain appropriate information of evapotranspiration spatially and temporally, in Sardon catchment area The overestimation of evapotranspiration obtained by remote sensing approach found earlier in Sardon (Worku, 2000) occurs also in similar areas characterized by water limited environment and sparse vegetation area (Gokmen et al., 2011). It is also not known how the remote sensing approach compares with hydrological model simulation approach in obtaining the value of actual evapotranspiration in the typically dry area of Sardon catchment area.

1.3. Research identification

1.3.1. Research objectives

General objective

To compare the ability of two different approaches; remote sensing approach and hydrological model simulation approach, to estimate evapotranspiration in dry climate area.

Specific objective

1. To estimate evapotranspiration using remote sensing approach.
2. To estimate evapotranspiration using hydrological model simulation based on ground measurement data.
3. To compare the two results of evapotranspiration.
4. To validate the two results of estimated evapotranspiration using eddy covariance calculation method

1.3.2. Research questions

1. What is the amount of evapotranspiration of the two different applying methods?
2. What is the correlation of the result of evapotranspiration estimated of the two different methods?
3. What is the accuracy of the two evapotranspiration estimates as compared to the evapotranspiration using eddy covariance method?

1.4. Organization of the thesis

The thesis is organized in seven chapters. The content is outlined as follows:

Chapter 1 Introduction

Chapter 2 Theoretical background

Chapter 3 Study area

Chapter 4 Materials and data collection

Chapter 5 Methods

Chapter 6 Results and discussion

Chapter 7 Conclusions and Recommendations

2. THEORETICAL BACKGROUND

Evapotranspiration is the combination of two separate processes; evaporation and transpiration. Evaporation is the conversion process from liquid water to water vapour and then it's removed from the evaporating surface. Evaporation can take place from different sources: open water, soil pores, intercepted water on leaves and other surfaces. Meanwhile, transpiration is the biological driver evaporation of water from leaves, stem, or root of the plants.

In the hydrologic terminology, total evapotranspiration consists of surface evapotranspiration *(ET_s)* and subsurface evapotranspiration *(ET_{ss})* which itself consists of unsaturated evapotranspiration *(ET_u)* and groundwater evapotranspiration *(ET_g)*(Lubczynski, 2011)

$$ET = ET_s + ET_{ss} = ET_s + (ET_u + ET_g) \qquad \textit{Equation 1}$$

$$ET_u = E_u + T_u \qquad \textit{Equation 2}$$

$$ET_g = E_g + T_g \qquad \textit{Equation 3}$$

In general, evapotranspiration can be distinguished between potential evapotranspiration (PET) and actual evapotranspiration (AET). Thornthwaite (1984) defined potential evapotranspiration as the amount of water which would transpire and evaporate if it were available (in: Lhomme, 1997), Whereas, Brutsaert (1982) also referred to by Lhomme (1997), defined potential evapotranspiration as "the maximum rate of evapotranspiration from a large area covered completely and uniformly by an actively growing vegetation with adequate moisture at all times". Actual evapotranspiration can be defined as the real amount of water consumed by the soil and vegetation.

Land-based data, satellite data, and computer models are different approaches to explain the complex time and space variations of physical processes produced by the climate system and the hydrologic cycle (Shelton, 2008). Gieske (2003) reviewed some generally applied methods for monitoring evapotranspiration (actual evapotranspiration) on global, regional and local scales. The methods can be grouped as: remote sensing, hydrological modelling and direct measurement approach.

In the following sections, these methods are explained. The calculation of potential evapotranspiration is also explained as it is input for the hydrological model.

2.1. Remote sensing approach

In Kalma et al (2008), some methods of estimating evapotranspiration using remote sensing data are reviewed. These methods are based on the concept of the surface energy balance. This approach provides the technique of measuring the thermal infrared, near infrared and visible bands of remote sensing data as input for parameterization of the energy balance components in *ET* calculation. This technique is able to measure repeatedly the same area with large coverage and on pixel-based discretization.

The surface energy balance which can governs evapotranspiration process is commonly written as :

$$R_n = G_0 + H + \lambda E \qquad \textit{Equation 4}$$

Where, R_n is the net radiation flux at the surface [W.m^{-2}], G is the soil heat flux [W.m^{-2}], H is the sensible heat flux to the air [W.m^{-2}], and λE is the turbulent latent heat flux [W.m^{-2}].

Net radiation (R_n) as the result of net shortwave and long wave radiation can be expressed mathematically as:

$$R_n = (1-\alpha).R_{swd} + \varepsilon.R_{lwd} - \varepsilon.\sigma.T_0{}^4 \qquad \textit{Equation 5}$$

where α is the albedo, R_{swd} is the downward solar radiation [W.m^{-2}], R_{lwd} is the downward long wave radiation [W.m^{-2}], ε is the emissivity of the surface, σ is the Stefan-Bolzmann constant [Jm^{2}s^{-1}K^{-4}], and T_0 is the surface temperature [K].

From *Equation 4*, remote sensing-based evapotranspiration rates (λE) are calculated as the residual in the surface energy balance equation.

$$\lambda E = R_n - H - G_0 \qquad \textit{Equation 6}$$

The estimation of sensible heat flux is the most difficult part because of the dependence on the aerodynamic resistance. The sensible heat flux (H) is calculated by the bulk transfer equation:

$$H = \rho C_p \frac{(T_0 - T_a)}{r_a} \qquad \textit{Equation 7}$$

Where ρ and C_p are constant values (respectively, air density and specific heat) (J m^{-3} ^{0}C^{-1}) and T_0 and Ta being surface and air temperature (^{0}C) r_a is the aerodynamic resistance to sensible heat transfer between the surface and height, which depends on stability and H itself (see *Section 2.1.1.2*).

In terms of remote sensing, T_0 is land surface temperature (LST) that can be retrieved from thermal band of satellite image. LST is an important factor in controlling chemical, biological and most physical data, which is controlled by the surface energy balance, atmospheric state, thermal properties of the surface, and also subsurface mediums (Becker & Li, 1990).

SEBS is a remote sensing model which has been proposes for the estimation of atmospheric turbulent fluxes and evaporative fraction using satellite earth observation data, in combination with meteorological information at proper scales (Su, 2002).

2.1.1. Surface Energy Balance System (SEBS) algorithm

In SEBS, the estimation of atmospheric turbulent fluxes using satellite earth observation data is formulated coherently. The advance algorithm is designed for composite terrain at a larger scale with heterogeneous surfaces. In estimating the surface heat flux, SEBS model considers the dry-limit and wet-limit conditions which are used to estimate the upper and lower boundary of sensible heat flux.

2.1.1.1. Soil heat flux

The equation for calculating soil heat flux (G) can be parameterized as:

$$G = R_n.[\Gamma_c + (1-f_c).(\Gamma_s - \Gamma_c)] \qquad \textit{Equation 8}$$

The ratio of soil heat flux to net radiation for fully vegetated surface; Γ_c = 0.05 and bare soil; Γ_s = 0.315 are constant. A linear interpolation can be performed between these limiting cases using the fractional canopy coverage *(f_c)*. Fractional canopy coverage can be determined using several methods using remote sensing data.

2.1.1.2. Sensible heat flux

The evaluation of sensible heat flux (H) is the most important in the SEBS algorithm. Sensible heat flux is calculated using Monin-Obukhov Similarity (MOS) theory. Within the Atmospheric Surface Layer (ASL), the bottom of the Atmospheric Boundary Layer (ABL) and above the roughness sub layer, the governing equation for mean wind and temperature profiles (T_0-T_a) can be expressed as:

$$u = \frac{u^*}{k}\left[ln\left(\frac{z-d_0}{z_{0m}}\right) - \Psi_m\left(\frac{z-d_0}{L}\right) + \Psi_m\left(\frac{z_{0m}}{L}\right)\right] \quad \textit{Equation 9}$$

$$T_0 - T_a = \frac{H}{ku^*\rho C_\rho}\left[ln\left(\frac{z-d_0}{z_{oh}}\right) - \Psi_h\left(\frac{z-d_0}{L}\right) + \Psi_h\left(\frac{z_{0h}}{L}\right)\right] \quad \textit{Equation 10}$$

From Sensible heat flux *(H)* estimated in ***Equation 7*** and ***Equation 10*** for ($T_0 - T_a$)*;* the aerodynamic resistance (r_a) can be defined as:

$$r_a = \frac{1}{ku^*}\left[ln\left(\frac{z-d_0}{z_{oh}}\right) - \Psi_h\left(\frac{z-d_0}{L}\right) + \Psi_h\left(\frac{z_{0h}}{L}\right)\right] \quad \textit{Equation 11}$$

With, u and u^* are the average wind speed and wind friction velocity, k is von Karman's constant, d_0 is the zero plane displacement height, z_{0m} and z_{0h} are the roughness for momentum and heat transfer respectively, Ψ_m and Ψ_h are stability correction functions for momentum and heat transfer respectively, ρ and C_ρ are air density and specific heat correspondingly and L is the Obukhov length which is expressed as :

$$L = -\frac{\rho C_\rho u_*^3 T_v}{kgH} \quad \textit{Equation 12}$$

Where T_v is the virtual potential temperature near the land surface and g is the acceleration due to the gravity.

The actual sensible heat flux resulted by ***Equation 7*** is constrained by the sensible heat flux at the wet limit H_{wet}, and the sensible heat flux at the dry limit H_{dry}. Under dry-limit condition, latent heat will be zero due to the limitation of soil moisture which means that the sensible heat flux will be in maximum value. At this condition, the sensible heat flux can be calculated as:

$$\lambda E_{dry} = R_n - G_0 - H_{dry} = 0, or \quad \textit{Equation 13}$$

$$H_{dry} = R_n - G_0 \quad \textit{Equation 14}$$

In the wet-limit condition, the latent heat flux will take place at potential rate, and the sensible heat flux will be in minimum value but not zero.

$$\lambda E_{wet} = R_n - G_0 - H_{wet}, or \quad \textit{Equation 15}$$

$$H_{wet} = R_n - G_0 - \lambda E_{wet} \quad \textit{Equation 16}$$

2.1.1.3. Evaporative fraction and actual evapotranspiration

In SEBS, evaporative fraction is estimated by determining dry and wet limits of sensible heat flux. From the two conditions of sensible heat flux, the relative evaporation can be evaluated with the following equation:

$$\Lambda_r = \frac{\lambda E}{\lambda E_{wet}} = 1 - \frac{\lambda E_{wet} - \lambda E}{\lambda E_{wet}} = 1 - \frac{H - H_{wet}}{H_{dry} - H_{wet}} \quad \textit{Equation 17}$$

Finally, the evaporative fraction is defined by the following equation:

$$\Lambda = \frac{\lambda E}{H + \lambda E} = \frac{\lambda E}{R_n - G} = \frac{\Lambda_r . \lambda E_{wet}}{R_n - G} \quad \textit{Equation 18}$$

Once that the evaporative fraction is defined, the daily evapotranspiration can be determined as :

$$AET = 8.64x10^7 x \frac{\Lambda.R_{n\,day}}{\lambda\rho_w}$$ *Equation 19*

AET is daily mean evapotranspiration [mm.d^{-1}], ρ_w is density water [kg.m^{-3}], and Λ is daily evaporative fraction, which is assumed equal to the instantaneous value, and $R_{n\,day}$ is the daily average net radiation [W.m^{-2}].

2.2. Hydrological model simulation approach

A number of hydrological models were developed in the past to solve the water balance for given areas. These models varies in complexity going from simple analytical models to complex systems of differential equation solved with numerical model implemented in computer programs.

This approach indirectly estimates evapotranspiration; integrating ground measurement data and model simulation. HYDRUS 1D version 4 software package was used for the estimation of ET. HYDRUS 1D is an unsaturated zone modelling package that can be used to simulate the one-dimensional movement of water, heat and multiple solutes in variably saturated media. Insitu data are used to model the soil profile in HYDRUS 1D and estimate ET simulating the flow of water in the soil (Šimůnek et al., 2009).

2.2.1. Uniform water flow

HYDRUS solves Richards's equation numerically and simulates water flow in the vadose zone. Developed by Lorenzo A. Richard (Richards, 1931), the equation describes the water movement through the vadose zone of the soils. Richard's equation is the foundation of all mechanistic models used to simulate the dynamics of water in permeable materials (aquifers).

For uniform water flow, the modified form of the Richard equation assumes the assumption that the air phase plays an insignificant role in the liquid flow process and that water flow due to thermal gradients can be neglected.

$$\frac{\partial\theta}{\partial t} = \frac{\partial}{\partial x}\left[K\left(\frac{\partial h}{\partial x} + cos(\alpha)\right)\right] - S$$ *Equation 20*

Where h is the power pressure head [L], θ is the volumetric water content [L^{3}L^{-3}], t is time [T], x is the spatial coordinate [L] (positive upward), S is the sink term [L^{3}L^{-3}T^{-1}], α is the angle between the flow direction and the vertical axis, and K is the unsaturated hydraulic conductivity.

$$K\,(h.x) = K_s(x)K_r(h,x)$$ *Equation 21*

K_r is the relative hydraulic conductivity [-], and K_s is the saturated hydraulic conductivity [LT^{-1}]

2.2.2. Initial and boundary conditions

The initial condition required by the model is the pressure head profile in the soil (Equation 22).

$$h(x,t) = h_i(x) \qquad t = t_0$$ *Equation 22*

h_I *(L)* is a prescribed function of x, and t_0 is the time when the simulation begins.

The following boundary conditions are used in HYDRUS 1D. The conditions must be specified at the soil surface (*x=L*) or at the bottom of the soil profile (*x=0*).

$$h(x,t) = h_i(x) \qquad at\ x = 0\ or\ x = L$$ *Equation 23*

$$-K\left(\frac{\partial h}{\partial x} + cos\,\alpha\right) = q_0(t) \qquad at\ x = 0\ or\ x = L$$ *Equation 24*

$$\frac{\partial h}{\partial x} = 0 \qquad at\ x = 0 \qquad \text{Equation 25}$$

Where, h_o (L) and q_o (LT^{-1}) are the prescribed values of the pressure head and the soil water flux at the boundary, respectively.

2.3. Direct measurement approach

Direct measurement is a category of measuring when all the output is provided by the measuring instrument. In estimating evapotranspiration, eddy covariance method is one important approach which has been used extensively. This method is a powerful tool to validate remote sensing method which estimate evapotranspiration; the error bound of flux tower measurement is about 20 – 30 % (Glenn et al., 2007).

2.3.1. Eddy covariance method

Eddy covariance is a technique which can be applied for direct measurement of evapotranspiration. Eddy covariance is a micrometeorological technique which can estimate water vapour and heat fluxes by measuring the fluctuations in wind speed, vapour density and air temperature in a variety of ecology and farmland systems (Ding et al., 2010).

The concept of eddy covariance is the measurement of heat (λE and H) and mass (CO_2, H_2O, other species) exchange by high frequency measurements of atmospheric turbulence and concentration. Eddy covariance measurement requires not only sufficiently large homogeneous surface, net advection of heat or mass, but also sufficient turbulence (Purba & Anderson, 2005).

In the atmospheric boundary layer (ABL); the lower part of the atmosphere, the dominant transport mechanism is turbulence. Turbulence can be classified from its driving source; thermal turbulence and mechanical turbulence. Thermal turbulence is a result of the air heating which forces thermal bubbles to be formed and rise up. Mechanical turbulence resulted from wind shear that stems from frictional drag. Fractional drag formed when ground air flow is hampered by the variety of obstacles.

Foken (2008) referred by Rwasoka (2010) define the general framework of covariance as :

$$\overline{w'x'} = \frac{1}{N-1}\sum_{k=0}^{N-1}\left[(w_k - \overline{w_k})(x_k - \overline{x_k})\right] \qquad \text{Equation 26}$$

Where w is the vertical velocity and x is a scalar or any two horizontal wind components. Sensible heat heat flux (H) and latent heat flux (λE) (in Wm^{-2}) are calculated using the following equations:

$$H = \rho_a . C_p . \overline{w'T'} \qquad \text{Equation 27}$$

$$\lambda E = \lambda \frac{M_a/M_w}{P} \rho_a \overline{w'e'} \qquad \text{Equation 28}$$

Where, ρ_a is density of air, w' is the turbulent vertical velocity [$m.s^{-1}$]. T' is the deviation in temperature [K] and C_p being the specific heat capacity [J kg K^{-1}].

In calculating evapotranspiration, the covariance of vertical wind speed (w') and specific humidity (q') in kg H_20 (kg air)$^{-1}$ are used as the following equation:

$$E = \rho_a . \overline{w'q'} \qquad \text{Equation 29}$$

With, ρ_a as density of air (g m^{-3}) and E is evaporation in kg m^{-2} s^{-1} or mm s^{-1}.

2.3.2. Eddy flux footprint

A footprint is the relative contribution from each element of the surface area source to the flux at measurement height (Vesala et al., 2008). Determination of the flux footprint is important as micrometeorological techniques in estimating surface fluxes from horizontally sources (Horst & Weil, 1992). The source areas (footprint) of eddy flux measurements have different size and directionality through time based on the micrometeorological data of the flux tower (Detto et al., 2006).

Models for estimating the footprint can be classified into four different approaches: (i) analytical models, (ii) Langrangian stochastic particle dispersion models, (iii) large-eddy simulations, and (iv) closure models. Vesala et al (2008) in their paper, reviewed the footprint modelling; the theoretical background, the most successful modelling approaches and the relationship with flux measurements. Hsieh et al (2000) developed a new analytical model for footprint estimation. They described an approximation analytical expression and the relationship between footprint, observation height surface roughness, and atmospheric stability.

2.4. Potential evapotranspiration

From the meteorological data of eddy tower, potential evapotranspiration had been estimated using Penman-Monteith (PM) and Priestley-Taylor (PT) calculation method.

2.4.1. Penman-Monteith (PM) evapotranspiration

The PM equation introduce a composited plant stomata resistance to vapour transport through a bulk surface resistance (Monteith, 1965) as referred in the paper of Sumner and Jacobs (2005). The potential evapotranspiration of Penman-Monteith is expressed as λE, as the following equation:

$$\lambda E = \frac{\Delta(R_n - G) + \rho_a c_p (e_s - e)/r_a}{\Delta + \gamma(1 + r_s/r_a)} \qquad \textit{Equation 30}$$

Where Δ is the slope of the vapour pressure curve [hPaK^{-1}], $(e_s\text{-}e)$ is the vapour pressure deficit [kPa]; e_s is the saturation on vapour pressure of the air [kPa], e is the actual vapour pressure of the air [kPa], γ is the psychometric constant, r_s is surface resistance [ms^{-1}], r_a is aerodynamic resistance [ms^{-1}].

The aerodynamic resistance is estimated using Monin-Obukhov similarity and assuming neutral condition and is expressed with the following equation:

$$r_a = \frac{ln[(z-d)/z_0].ln[(z-d)/z_{ov}]}{k^2 u} \qquad \textit{Equation 31}$$

z is the height at which wind speed is measured [m], d is the height of displacement [m], z_0 is roughness height for momentum [m], z_{ov} is roughness height for water vapour [m], k is von Karman's constant, equal to 0.41, and u is the horizontal wind speed at sensor height z [ms^{-1}].

2.4.2. Priestley-Taylor (PT) evapotranspiration

The Priestley-Taylor approach is a simplification of the Penmann-Monteith equation in calculating evapotranspiration. It is described as:

$$\lambda E = \alpha \frac{\Delta}{\Delta + \gamma}(R_n - G) \qquad \textit{Equation 32}$$

Where α is an empirically determined dimensionless correction, α = 1.26. The other variables are previously defined.

3. STUDY AREA

3.1. Location

The study area is part of Sardon Catchment, which is situated in Salamanca Province, central-western Spain (Figure 3-1). Geographically, the study area is located between longitudes from 738664.4 to 740984.9 W and latitudes from 4554554.4 to 4556115.0 N.

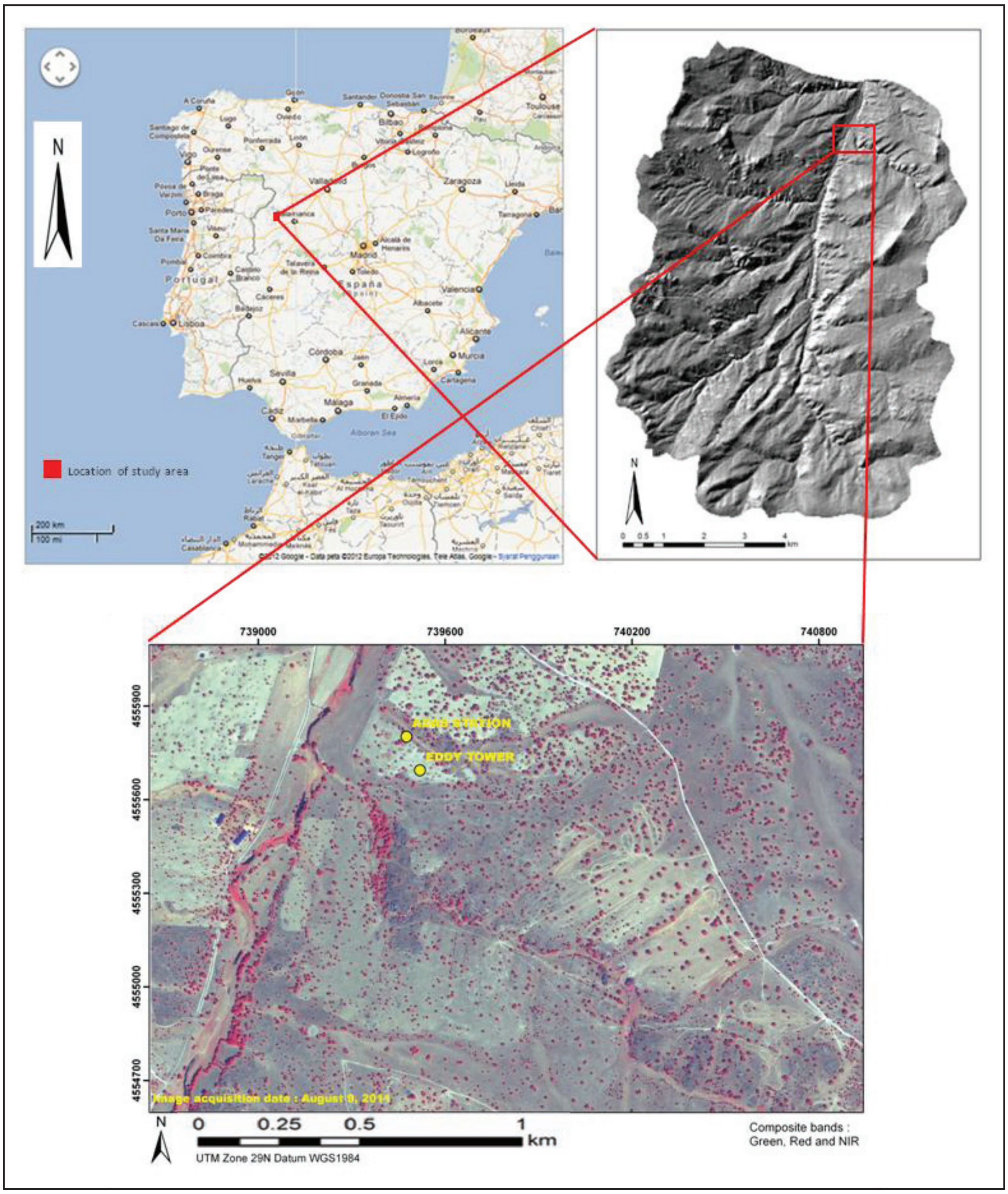

Figure 3-1: Maps showing location of the study area
(*map source : (1) http://maps.google.com/ (2) SRTM DEM, and (3) Quickbird Image*)

3.2. Climate settings

The study area selected for conducting the research has a typical semi-arid climate. Semi-arid climate areas are defined by Köppen classification as the (non-polar) areas which receiving low annual rainfall (less than 500 mm) and generally has short-grass or scrub vegetation (Peel et al., 2007).

The rainfall events for the two observation years are slightly different (Figure 3-2). The precipitation in 2010 is higher than in 2009, especially in the two dry months on which the study was focused; July and August.

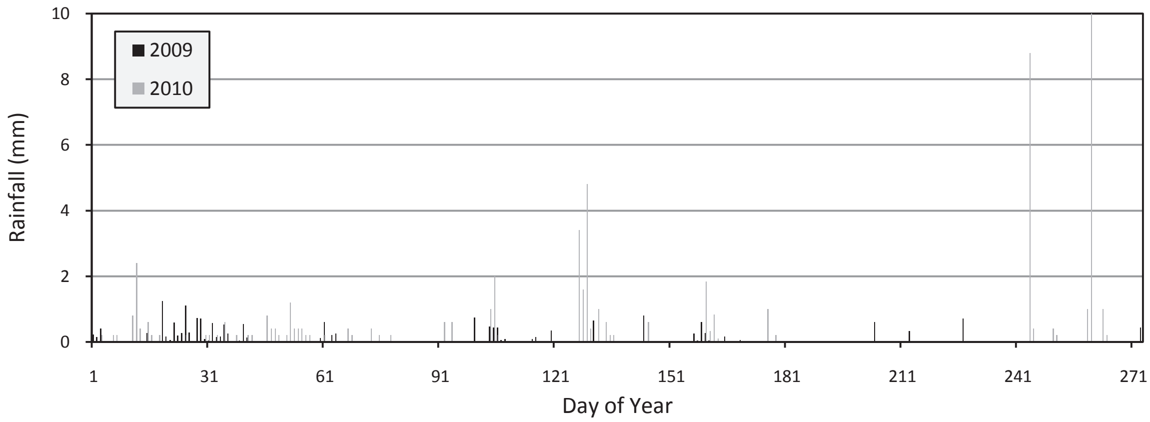

Figure 3-2: Rainfall in study area for 2009-2010

Based on the temperature variations, the average temperature of the hottest month (August) is less than 22^0 C and the four months average temperature is more than 10^0 C, the study area is classified as *Moderate Summer (Peel et al., 2007)*.

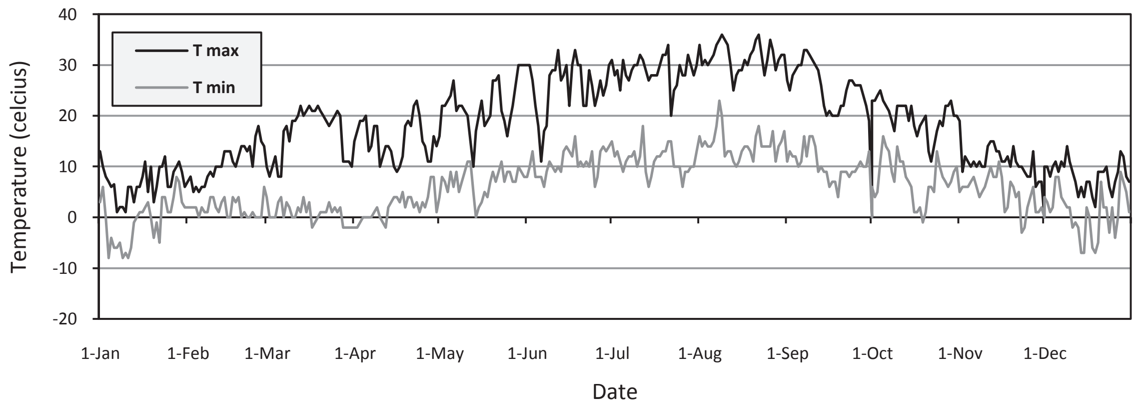

Figure 3-3: Temperature in study area for 2009

3.3. Topography and drainage

The study area has a very gentle undulating topography which controlled by geological structure and subsequent interactive weathering processes. In some higher relief, the area is comprised by quartzite dykes, massive and fractured granitic outcrop with large boulders and capped by thin insitu overburden. The elevation of the study area varies from 760 to 797 meters above mean sea level (m amsl).

The study area is part of Sardon catchment with Sardon River as the main stream. The drainage network in Sardon Catchment is mainly described as a numerous stream system, mostly influenced by the intermittent regime of Sardon River. The intermittent stream can be defined as a stream where flow is present only for part of the time, usually after rainstorm, during wet weather, or for only part of the year. Run off from rainfall is the main source for stream flow, therefore during dry periods these stream would not have flowing water. Due to the thin highly-permeable upper unconsolidated layer which is typical in semi-arid area with hard rock, the run-off system of the study area is characterized by low retention capacity.

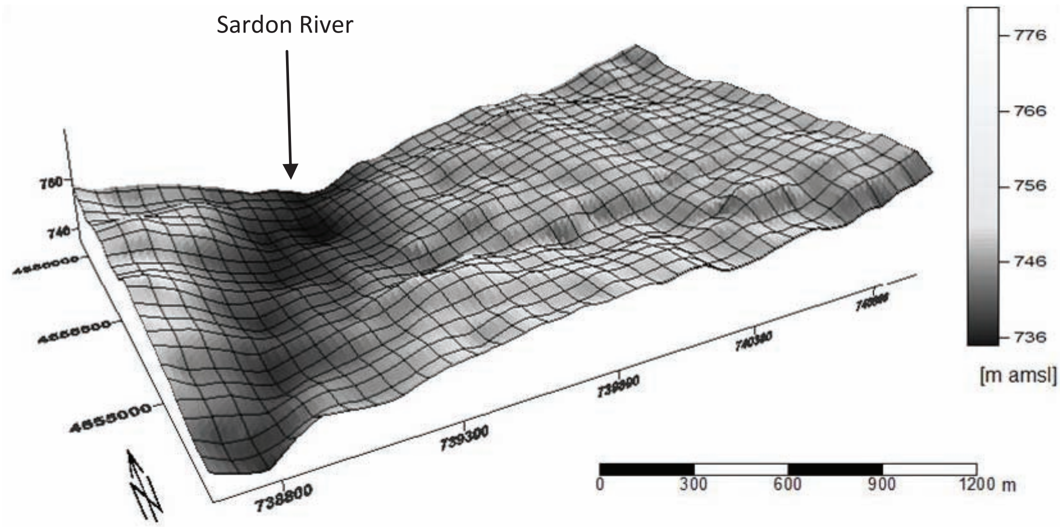

Figure 3-4: 3-D visualisation showing the topography of study area

4. MATERIALS AND DATA COLLECTION

4.1. Meteorological data

Meteorological data is an important input for the two approaches: remote sensing and hydrological model simulation. These data based on the two instrument towers which are located in the study area (Table 4-1).

Table 4-1: The two towers in the study area

Tower	Reference height (meter)	Coordinates (UTM, ED 1950)	
		X	Y
ADAS Station	6	739476	4555802
Eddy tower	10	739519	4555694

The Automated Data Acquisition Systems (ADAS) is a remotely controlled system consists of sensors monitoring hydrological variables, and some loggers for managing the performance of the sensor with digital format output (Lubczynski & Gurwin, 2005). The Eddy Tower is a set of instrument for measuring turbulent heat fluxes, net radiation and meteorological variables. The variables measured by the instrument of the Eddy Tower are presented in Table 4-2.

Table 4-2: The instrument of the Eddy Tower

Instrument	Height (meter)	Thematic class	variables
3-D CSAT (Campbell Scientific)	10	10 Hz Turbulence data sonic temperature (Ts)	U_x, U_y, U_z, T_s
Licor 7500 Gas Analyzer	10	Gas concentrations	Conc. H_2O
CNR 1 Net Radiometer (Kipp and Zonen)	10	Net radiations (R_n budget)	SW↓, SW↑, LW↓, LW↑, and R_{sensor}
Hukseflux Plates (2 plates)	-0.01	Soil heat flux (set up 1)	SHF 1 and SHF 2
TCAF sensors (Campbell Scientific) 3 and 7 cm and a Hukseflux plate	-0.03 and -0.07 (TCAF) -0.10 (SHF3)	Soil heat flux (set up 2)	T_{3cm}, T_{7cm} and $SHF3_{10cm}$
Vaisala	10	Meteorological	Wind direction, RH, Temp


Figure 4-1: ADAS Station and the eddy tower in the study area

The data used for input parameters for SEBS analysis are in time of LANDSAT 5 TM overpass (local time/GMT+2), asTable 4-3.

Table 4-3: Meteorological data of LANDSAT 5 TM overpass for SEBS input

Year	Date	Hour	Wind speed	Air temperature	Air pressure	Relative humidity	Incoming shortwave
			($m.s^{-1}$)	(Celsius)	(hpa)	(%)	(Wm^{-2})
2009	21-Aug	12.52	1.853	20.61	932	66.53	814.0
	6-Sep	12.52	1.557	21.43	934	35.18	779.4
2010	16-Jul	12.52	3.438	21.40	933	51.87	828.2
	1-Aug	12.52	4.804	28.30	930	22.32	821.0

4.2. LANDSAT 5 TM images

4.2.1. Introduction of TM LANDSAT images

The Thematic Mapper (TM) is the advance multispectral scanner of LANDSAT. It is a sensor designed to achieve higher image resolution, sharper spectral separation, improved geometric fidelity and greater radiometric accuracy. LANDSAT 5 was launched by NASA on 1st March 1984. It carried the two instruments; Multispectral Scanner System (MSS) and Thematic Mapper (TM). The MSS instrument was turned off in August 1995, but the TM instrument is still in normal operation.

LANDSAT 5 TM instrument measures in 7 bands simultaneously. A TM scene has an *Instantaneous Field Of View* (IFOV) of 30 square meters in bands 1-5 and 7 while band 6 has an IFOV of 120 square meters on the ground (http://www.ldcm.nasa.gov/about/tm.html). Spatial and spectral characteristics of these bands are shown in Table 4-4.

Table 4-4: Spatial and spectral characteristic of LANDSAT 5 TM

Band no.	Spectral range (µm)	Ground resolution (m)
1	0.450 to 0.520	30
2	0.520 to 0.600	30
3	0.630 to 0.690	30
4	0.775 to 0.900	30
5	1.550 to 1.750	30
6	10.40 to 12.50	120
7	2.080 to 2.350	30

LANDSAT 5 TM is corrected using Standard Terrain Correction (Level 1T-precision and terrain correction). This correction type provides systematic radiometric and geometric accuracy by incorporating ground control points while employing a Digital Elevation Model (DEM) for topographic accuracy.

LANDSAT 5 TM is a standard product which was processed using Level 1 Product Generation System (LPGS) with the characteristic as shown in Table 4-5.

Table 4-5: Characteristic of LANDSAT 5 TM

Scene size	170 km x 185 km (106 mi x 115 mi)
Output format	Geo TIFF
Map projection	Universal Transverse Mercator (UTM)
Image orientation	MAP (North-up)
Resampling method	Cubic convolution (CC)

4.2.2. Image acquisition

The LANDSAT 5 TM images taken during the dry season of 2009 and 2010 were used for the study. The area of research is located in path 203 and row 31, and the metadata of the images are shown in Table 4-6. These images were downloaded from USGS portal (http://edcsns17.cr.usgs.gov).

Table 4-6: The LANDSAT 5 TM Images for the study

Date			Time overpass (GMT+0)	Image No.	Day of year
2009	August	21	10:56:56.9	LT52030312009233	233
	September	6	10:57:11.1	LT52030312009249	249
2010	July	16	10:52:15.7	LT52020322010197	197
	August	1	10:51:46.4	LT52020322010213	213

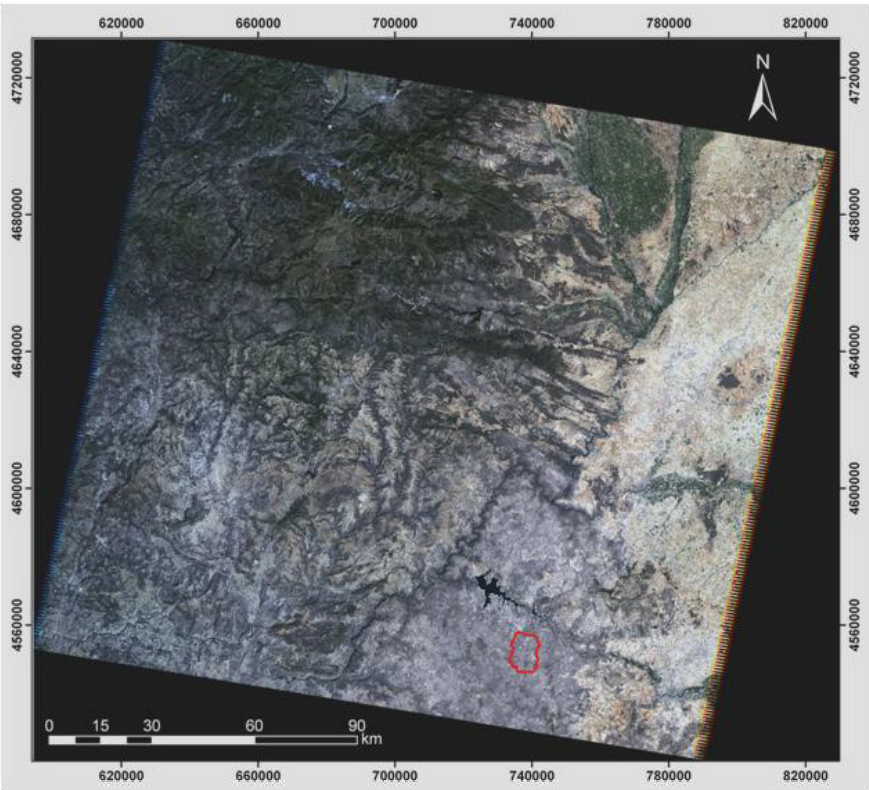

Figure 4-2: LANDSAT 5 TM scene of the study area in true colour composite, with the boundary of Sardon catchment.

4.2.3. Atmospheric correction

The accurate retrieval of surface reflectance and temperature is important in deriving land surface biophysical parameters and in determination of fluxes. Solar radiation passes through the atmosphere before it is collected by the instrument. Because of this, information of remote sensed imagery not only contains information about the earth's surface, but also information about the atmosphere. Therefore, removing the influence of the atmosphere is a critical pre-processing step in order to determine quantitative analysis of surface reflectance. To compensate for atmospheric effects, properties such as the amount of water vapour, scene visibility, and distribution of aerosols must be defined.

4.2.3.1. Atmospheric correction using FLAASH

Fast Line-of-sight Atmospheric Analysis of Spectral Hypercubes (FLAASH) was developed by spectral sciences, Inc, under the sponsorship of U.S. Air Force Research Laboratory. The first principle of FLAASH is that corrects wavelengths in the visible through near-infrared and shortwave infrared region, up to 3 μm. (ITT Visual Information Solutions, 2009). FLAASH is one atmospheric correction module which had been developed on ENVI. The parameter for ENVI FLAASH includes selecting of input radiance image, setting file defaults, entering information about the sensor and scene, selecting atmosphere and aerosol model, and setting for the atmosphere correction model.

FLAASH starts from a standard equation for spectral radiance at a sensor pixel, *L*, that applies to the solar wavelength range (thermal emission is neglected) and flat, Lambertian materials or their equivalents (Matthew et al., 2000). The equation is as follows:

$$L^* = \frac{A\rho}{1-\rho_e s} + \frac{B\rho_e}{1-\rho_e S} + L^*{}_a \qquad \textit{Equation 33}$$

Where :

- ρ is the pixel surface reflectance,
- ρ_e is an average surface reflectance for the pixel and a surrounding region,
- S is the spherical albedo of the atmosphere,
- L^*_a is the radiance backscattered by the atmosphere,
- A and B are coefficients that depend on atmospheric and geometric conditions but not on the surface.

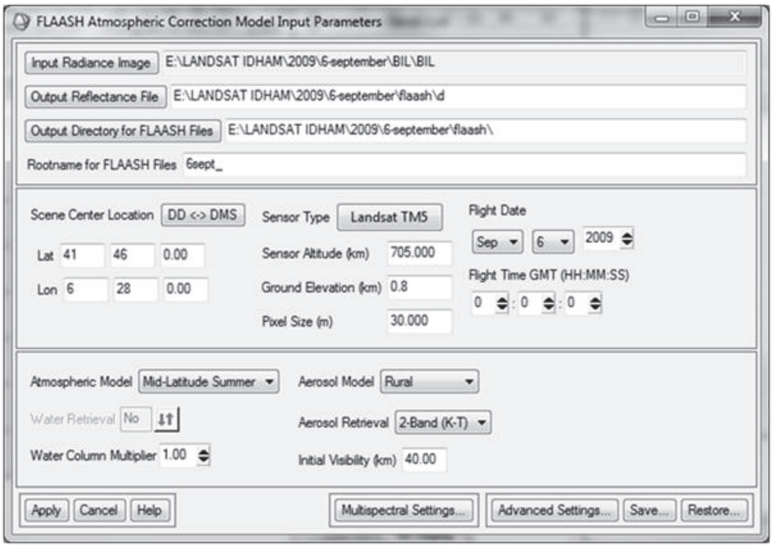

Figure 4-3: FLAASH atmospheric correction in ENVI-IDL

All the variables depend on the value of spectral channel. The correction can result a significant error of short wavelengths under hazy conditions.

The values of *A, B, S* and L_a are obtained from MODTRAN4 calculations, using the viewing and solar angles and the mean surface elevation of the measurement, and defining a certain model atmosphere, aerosol type, and visible range. The values of *A, B, S* and L_a are dependent on the water vapour column amount, which is generally not well known and may vary across the scene.

For LANDSAT which do not contains spectral channel in the appropriate wavelength conditions to support water retrieval, the column water vapour mount can be determined by a user-selected atmospheric model. This atmospheric model selection can produce more accurate corrections than using a constant water amount for the entire scene.

4.2.3.2. Atmospheric correction for thermal band

A lot of steps need to be carried out to access the accuracy of Land Surface Temperature retrieval from thermal data of satellite image. Sensor radiometric calibration and also atmospheric correction are important steps in this procedure. The effects which caused by absorption and emission by atmospheric vapour can cause significant errors in estimating surface temperature from remotely sensed thermal infrared data.

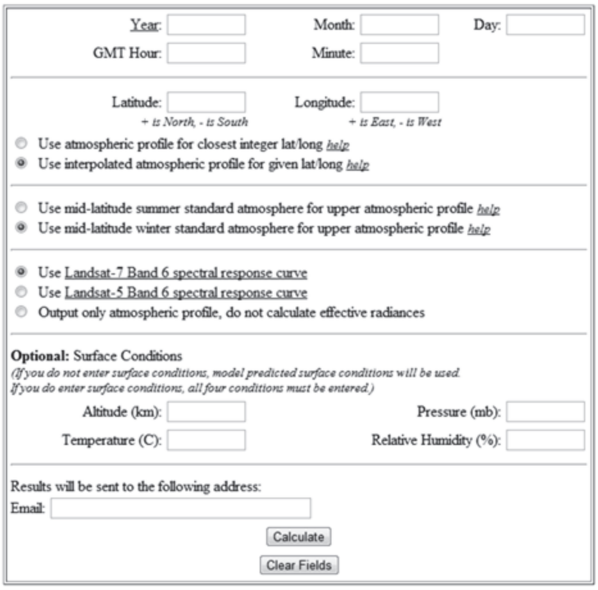

Figure 4-4: The Correction Parameter Calculator for LANDSAT

The LANDSAT production system is a product of NASA Earth Observation System which does not have derived physical parameters, such as surface temperatures. For retrieval surface temperature, NASA developed an atmospheric correction tool for public access for LANDSAT 5 TM. The tool, The Atmospheric Correction Parameter Calculator uses the National Centres for Environmental Prediction (NCEP) modelled atmospheric global profiles for a particular date, time and location as input. Using MODTRAN, the site specific atmospheric transmission and upwelling and down welling radiances are derived and applied to calculate an at-surface kinetic temperature for all the pixels in the scene of single thermal band (Barsi et al., 2005).

The parameters known will be used for converting space-reaching radiance to a surface-leaving radiance:

$$L_{TOA} = \tau \varepsilon L_T + L_u + \tau(1-\varepsilon)L_d \qquad \textit{Equation 34}$$

τ is the atmospheric transmission; ε is the emissivity of the surface, specific to the target type; L_T is the radiance of a blackbody target of kinetic temperature T; L_u is the upwelling or atmospheric path radiance; L_d is the down welling or sky radiance; and L_{TOA} is the space-reaching or TOA radiance measured by the instrument. The unit of radiance is in W/m^2.sr μm, and transmission and emissivity are unitless. The radiance temperature at the top of atmosphere is then calculated by the inversion of Plank's law, as the following equation :

$$T = \frac{k_2}{ln\left(\frac{k_1}{L_\lambda}+1\right)} \qquad \textit{Equation 35}$$

Where T is the radiance temperature; $L\lambda$ is spectral radiance in $Wm^{-2}sr^{-1}\mu m^{-1}$; k_1 and k_2 are the constant of calibration parameter.

Table 4-7: Constant of calibration parameter for LANDSAT

LANDSAT Sensor	k_1 [$Wm^{-2}sr^{-1}\mu m^{-1}$]	k_2 [K]
LANDSAT 7 ETM+	666.09	1282.71
LANDSAT 5 TM	607.76	1260.56

The brightness temperature from thermal band of LANDSAT can be expressed as :

$$B_6(T_6) = \tau_6[\varepsilon_6 B_6(T_s) + (1-\varepsilon_6)I_6^{\infty}] + I_6\downarrow \qquad \textit{Equation 36}$$

Where :

T_s = land surface temperature
T_6 = brightness temperature at band 6
τ_6 = atmospheric transmittance at band 6
ε_6 = surface emissivity
$B_6(T_6)$ = at-sensor registered radiance
I_6^{∞} = down welling radiance
$I_6^{\uparrow}$ = upwelling radiance

4.3. Field data collection and laboratory analysis

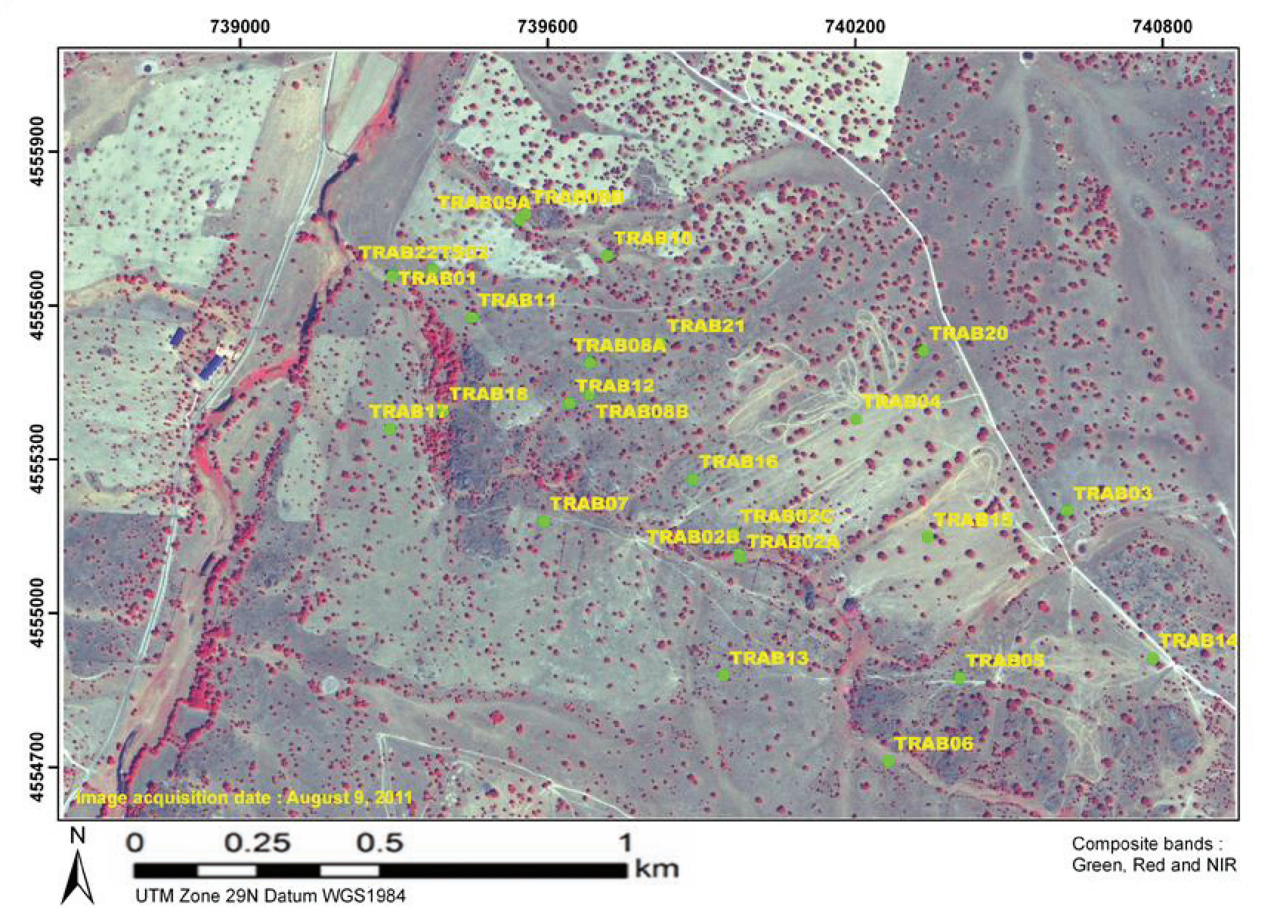

Figure 4-5: Distribution of augering location

In this study, field data collection is an essential part. This data is mainly required as input for HYDRUS 1D as a model. These data includes soil depth and the physical properties, water table depth and soil moisture. Soil sampling is also another task of this field work for laboratory analysis in order to obtain hydraulic properties of soils.

Soil sampling was carried out in the study area by hand augering process. The augering was spread over 26 locations in the study area (Figure 4-5). Depending on the total depth of each soil profile augering, one to four soil samples were collected at different depth in order to determine soil hydraulic properties of each depth. The soil samples were analysed in laboratory in several types of analysis.

Table 4-8: Location of the augering with number of samples

Object ID	GPS Coordinate		Total depth (cm)	Number of Samples		
	X	Y		Ring	Bag	Total
TRAB-01	739297	4555658	100	2	-	2
TRAB-02A	739977	4555107	100	1	1	2
TRAB-02B	739974	4555114	85	1	2	3
TRAB-02C	739964	4555155	25	-	1	1
TRAB-03	740614	4555199	13	-	1	1
TRAB-04	740202	4555378	23	-	1	1
TRAB-05	740404	4554873	76	1	1	2
TRAB-06	740265	4554711	230	-	6	6
TRAB-07	739593	4555179	93	1	-	1
TRAB-08A	739683	4555488	41	-	1	1
TRAB-08B	739682	4555426	40	-	-	0
TRAB-09A	739547	4555766	100	3	-	3
TRAB-09B	739557	4555777	100	-	2	2
TRAB-10	739717	4555697	125	2	1	3
TRAB-11	739453	4555576	93	1	-	1
TRAB-12	739643	4555409	97	-	-	0
TRAB-13	739944	4554878	16	-	1	1
TRAB-14	740782	4554912	60	-	1	1
TRAB-15	740342	4555148	33	-	1	1
TRAB-16	739884	4555261	50	-	1	1
TRAB-17	739293	4555359	24	-	1	1
TRAB-18	739396	4555393	100	2	-	2
TRAB-19	739283	4555580	19	-	1	1
TRAB-20	740333	4555511	33	-	1	1
TRAB-21	739821	4555526	13	-	1	1
TS-02	739376	4555669	25	3	6	9

Figure 4-6: Field data collection,
(1) Soil augering in TRAB 06 and (2) soil profile in TRAB 08

During fieldwork, observations of other important aspects such as field measurement documentation, and groundwater table observation on each augering points were also carried out.

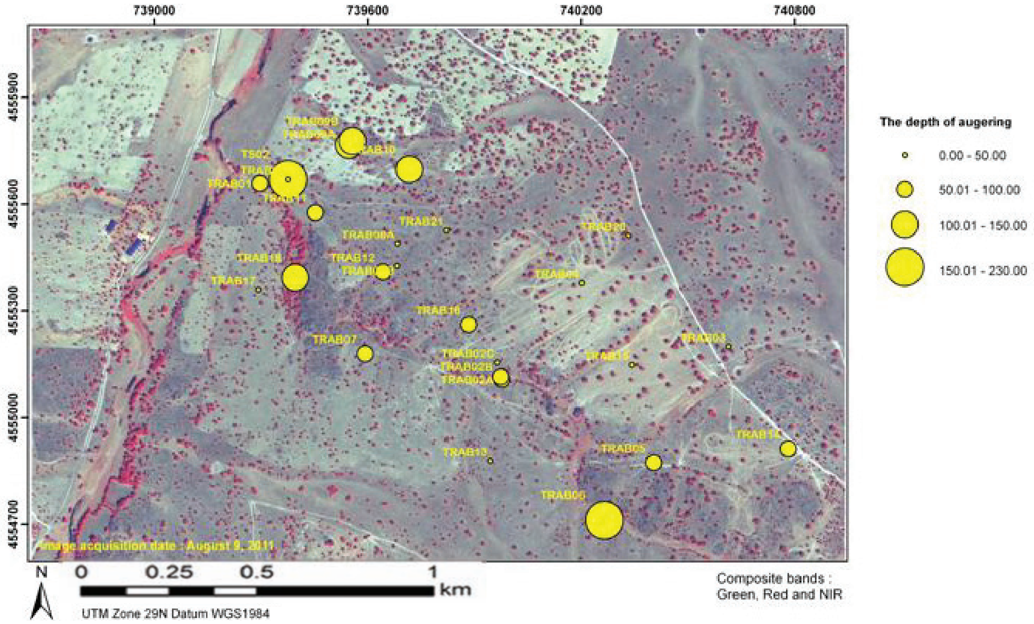

Figure 4-7: The depth of augering in measurement points

Soil samples collected from field were analyzed in laboratory to obtain its hydraulic parameter. The analysis methods conducted are:

- Particle size analysis

This method was used to obtain the soil texture, which is the proportioned weight of sand, silt and clay. The type of sample used for this analysis can be either bag sample or ring sample.

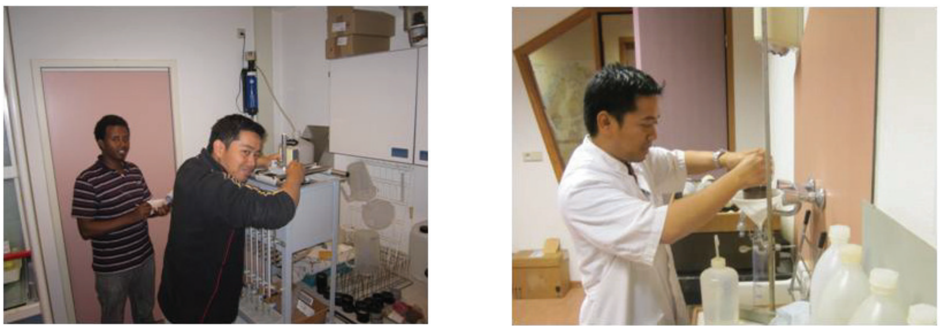

Figure 4-8: Some steps of laboratory analysis

- Permeameter test

It consists of constant head and falling head. These had been conducted to get the hydraulic conductivities of each sample soil. This analysis use only ring sample type.

Table 4-9: Types of laboratory analysis

Type of analysis	Number of samples
Particle size analysis	35 Samples
Permeameter test	
- Constant head	5 samples
- Falling head	9 samples

The result of each laboratory analysis is explained in *Chapter 6, Results and discussion.*

5. METHODS

5.1. General schematization

The general methodology of this study is schematically illustrated in Figure 5-1. The evapotranspiration value result obtained using two different approaches; remote sensing and hydrological model simulation, were compared with evapotranspiration from eddy covariance measurement.

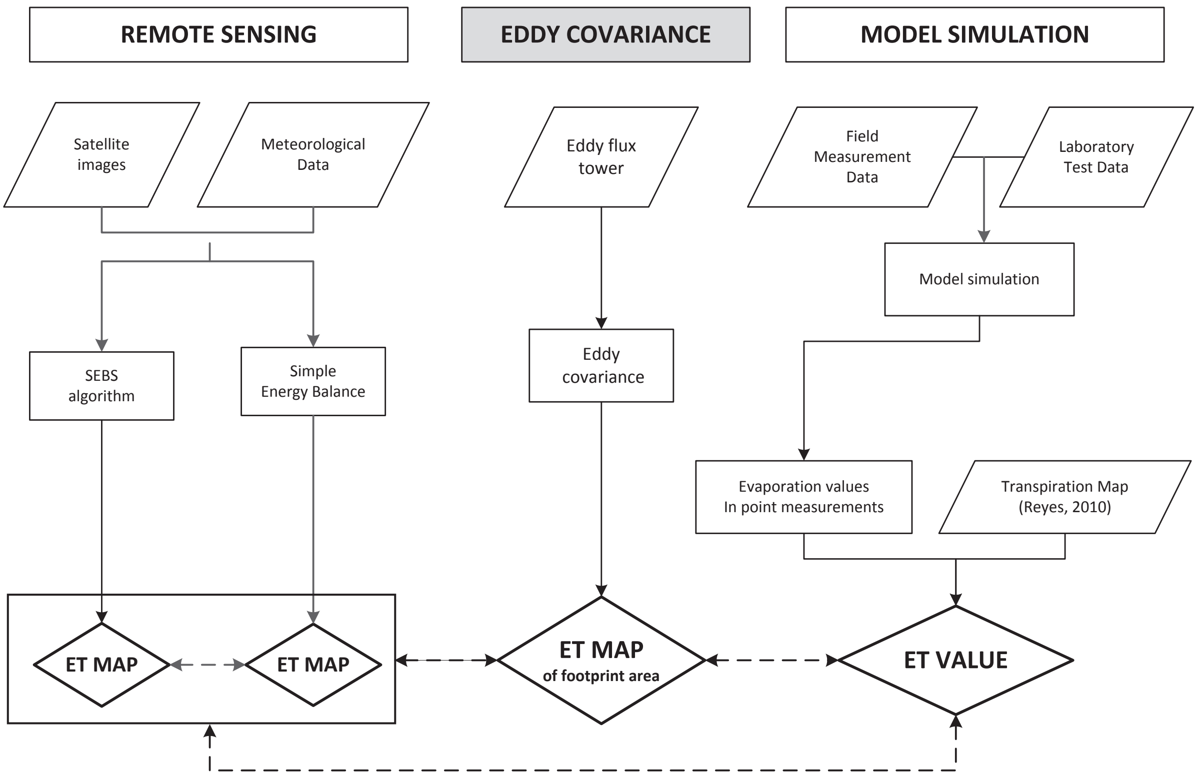

Figure 5-1: Flowchart showing the general methodology of the study

5.2. Remote sensing approach

In Figure 5-1, it is shown that there are two approaches in calculating ET in remote sensing approach, namely SEBS algorithm and Simple Energy Balance. SEBS is a model that requires a number of information whose collection is not straightforward (e.g. roughness length for momentum and heat, profiles within canopy wind, fractional vegetation cover and leaf area index) (Galleguillos et al., 2011). Nevertheless, the error probability may become larger when considering the typical sparse vegetation area in the study area.

A simple energy balance is an alternative model when the difference temperature is the most important parameter. This model can minimize error in data parameterization and LANDSAT TM is a sensor offers high quality spaceborne data of surface temperature which could be utilized well for applying this model.

5.2.1. SEBS algorithm

Algorithm of Surface Energy Balance System (SEBS) was applied as a model in the research area. The SEBS processing is implemented by ILWIS software, which can extract and process the remote sensing data and provide the outputs of energy balance, instantaneous actual evapotranspiration flux and daily evapotranspiration.

A SEBS is modelled for estimating atmospheric turbulent fluxes and evaporative fraction using satellite image as observation data, integrating with meteorological information. SEBS consists of a set of tools for determining the land surface physical parameters, such as surface albedo, emissivity, surface temperature and vegetation index from spectral reflectance and radiance measurements; a model for the determination of the roughness length for heat transfer; and a new formulation for the determination of the evaporative fraction on the basis of energy balance (Su, 2002). The conceptual scheme of the algorithm applied for this study is presented in Figure 5-2.

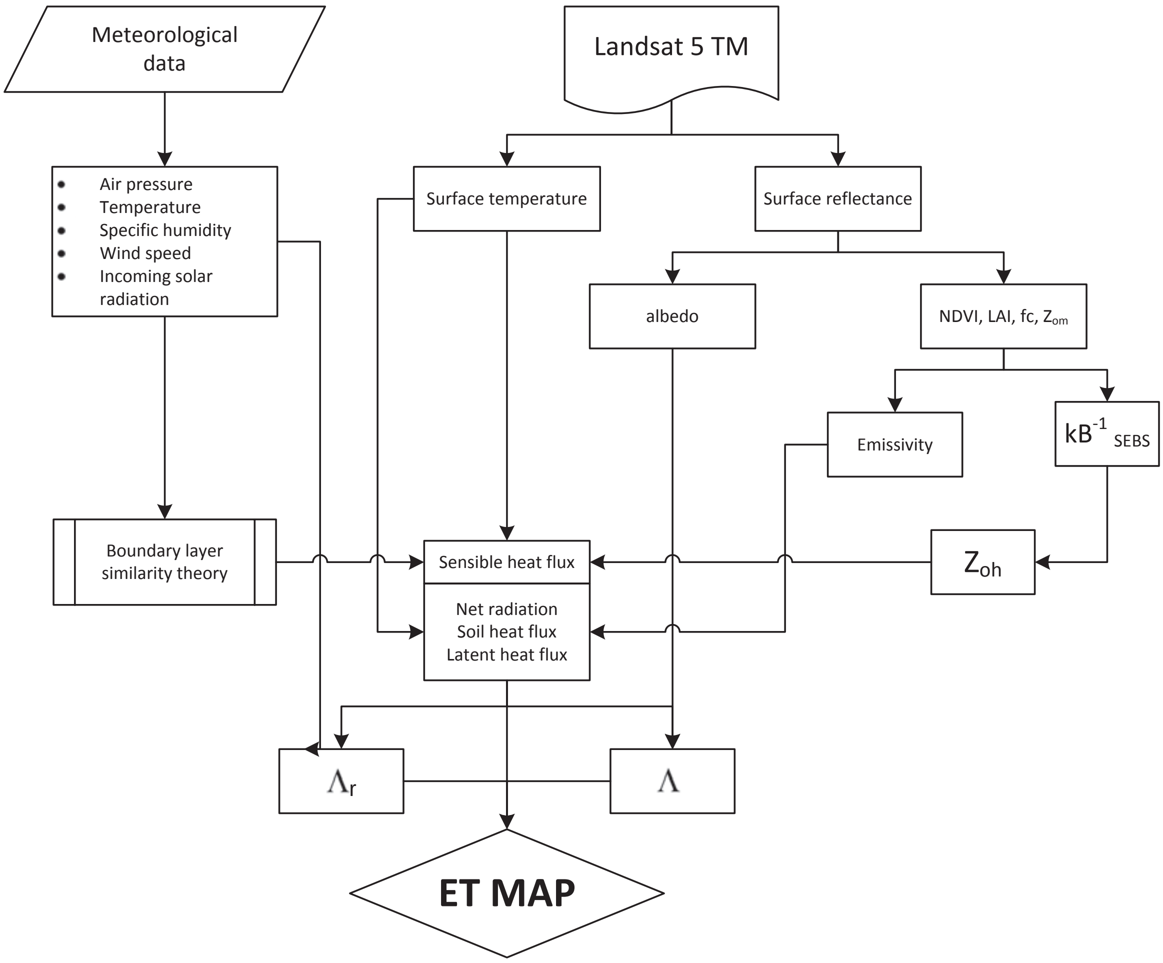

Figure 5-2: The conceptual scheme of SEBS algorithm

To apply SEBS, three sets of information as input are required, namely:

- The first set, consisting of land surface temperature, land surface emissivity, land surface albedo, fractional coverage and leaf area index, and the height of the vegetation (or roughness height), which could be derived from LANDSAT 5 TM imagery as remote sensing data.
- The second set, consisting of air pressure, humidity and wind speed at a reference height. The reference height is the measurement of each parameter in point application.

- The third set, which includes downward solar radiation, and downward long wave radiation which can be estimated from direct measurement, model output and parameterization.

5.2.1.1. Land surface temperature (LST)

Land surface temperature is one of the important core inputs for the SEBS model. Land surface temperature (LST) was retrieved by using *Equation 36,* in *Sub Chapter 4.2*.

5.2.1.2. Normalized difference vegetation index (NDVI)

NDVI is an index which shows the value of vegetation density and condition. It is an indicator for knowing the greenness of the land surface cover. NDVI is computed from the reflectance of the red and Near-infrared (NIR) channel as:

$$NDVI = \frac{\rho_{nir} - \rho_{red}}{\rho_{nir} + \rho_{red}} \qquad \text{Equation 37}$$

ρ_{nir} and ρ_{red} are atmospherically corrected reflectance of the near-infra red and the red bands respectively.

5.2.1.3. Fractional vegetation cover (f_c)

Fractional vegetation cover (f_c) is an important structural property of a plant canopy. f_c is related with the partition between soil and vegetation contribution for emissivity and temperature which is imperative for describing land surface process. Vegetation fraction has close relationship with NDVI, which is in SEBS land use automatic routines calculated as:

$$fc = \frac{(NDVI - NDVI_{min})^2}{(NDVI_{max} - NDVI_{min})^2} \qquad \text{Equation 38}$$

5.2.1.4. Land surface emissivity

Land surface emissivity is also a property of the land material where water content has an important role. In the relationship with the vegetation cover, Valor & Caselles (1996) derive the surface emissivity as the following equation:

$$\varepsilon_0 = \varepsilon_c f_c + \varepsilon_s (1 - f_c) + 4\langle d\varepsilon \rangle f_c (1 - f_c) \qquad \text{Equation 39}$$

Where, ε_c is emissivity of full vegetation cover, ε_s is emissivity of bare soil, f_c is the fractional vegetation cover, $d\varepsilon$ is the vegetation structure parameter. ε_c, ε_s, $d\varepsilon$ are taken as values 0.985, 0.96, 0.015 respectively.

5.2.1.5. Land surface albedo

Numerous studies had been developed in calculating the total shortwave broadband albedo from LANDSAT TM. Shunlin et al, (2001) developed a method for calculating land surface albedo from different sensors, including Thematic Mapper sensor. They provide conversion formulae for total broadband albedo: total visible albedo, diffuse albedo, total near IR albedo, and direct and diffuse near-IR albedo.

Duguay and LeDrew (1992) in Shunlin (2001) developed a linear formula using three LANDSAT TM bands, and resulted fits for all cover types well (*Equation 40*).

$$\alpha = 0.526\alpha_2 + 0.3139\alpha_4 + 0.112\alpha_7 \qquad \text{Equation 40}$$

5.2.1.6. Roughness length for heat and momentum transfer (Z_0h and Z_0m)

The roughness length for momentum (z_0m) and heat (z_0h) are required parameter for estimating sensible heat flux. In SEBS, the kB^{-1} model is used to estimate z_0m from z_0h. The relationship between z_0m and z_0h can be defined as:

$$z_{0h} = \frac{z_{0m}}{exp(kB^{-1})} \qquad \textit{Equation 41}$$

In this equation, kB^{-1} is the Stanton number, a dimensionless heat transfer coefficient. An extended model (Su et al. 2001 in (Su, 2002)) is proposed as follows :

$$kB^{-1} = \frac{kC_d}{4C_t\frac{u_*}{u(h)}\left(1-e^{-\frac{n_{ec}}{2}}\right)} fc^2 + 2f_cf_s\frac{k.^{u^*}/_{u(h)}.^{z_{0m}}/_h}{C^*t} + kB^{-1}{f_s}^2 \qquad \textit{Equation 42}$$

Where, f_c and f_s is the fractional canopy coverage and its complement. C_t is the heat transfer coefficient of the leaf. For most canopies and environmental conditions, C_t is bounded as 0.005N $\leq C_t \leq$0.075N (N is number of sides of a leaf to participate in heat exchange). The heat transfer coefficient of the soil is expressed as $Ct^* = Pr^{-2/3}/{R_e}^{*1/2}$, Pr is the Prandt number. The roughness Reynolds number can be estimated as ${R_e}^* = h_su^*/v$, where h_s the roughness height of the soil and v is the kinetic viscosity of the air which can be calculated as $v = 1.327.10^{-5}(p_0/p)(T.T_0)$, with p and T the ambient pressure and temperature and p_0 = 101.3 kPa and T_0 = 273.15 K.

For bare soil, kB^{-1} can be estimated according to Brutsaert (1982) in Su (2002), as :

$$kB^{-1} = 2.46({R_e}^*)^{1/4} - ln[7.4] \qquad \textit{Equation 43}$$

5.2.2. Simple energy balance method

In the SEBS algorithm part, the energy balance equation is explained *(Equation 4)*. The available net radiation is shared between soil heat flux (G) and sensible heat flux (H) and latent energy exchange (λE). In this algorithm, the aerodynamic resistance r_a between the surface and the reference height above the surface is used in sensible heat flux estimation, as expressed in *Equation 7* in page 4.

Simple energy balance is a simplified version method of surface energy balance approach in estimating actual ET. It is an extension method which is based on Surface Energy Balance Algorithm for Land (SEBAL) developed by Bastianseen (1998). The SEBAL is method which assumes that the temperature difference between the land surface and air near-surface temperature varies linearly with land surface temperature and derives this relationship based on two anchor pixels known as the hot and cold pixels. In SEBAL, the relationship between the near-surface temperature difference and the land surface temperature is used to estimate the sensible heat flux which varies as a function of the near-surface temperature difference, by assuming that the hot pixel experiences no latent heat; ET = 0.0, whereas the cold pixel can reach maximum ET.

Therefore, in Simple Energy Balance approach, actual ET was estimated by the near-surface temperature difference, which in turn is estimated from the land surface temperatures of the hottest pixel in the study area where is assumed that the latent heat flux is 0.

$$\lambda E = 0, \quad H = R_n - G \qquad \textit{Equation 44}$$

$$\rho C_p \frac{(LST - T_a)}{r_a} = R_n - G \qquad \textit{Equation 45}$$

$$r_a = \frac{LST - T_a}{(R_n - G).\rho C_p} \qquad \textit{Equation 46}$$

Another important assumption of this method is that the aerodynamic resistance (r_a) in the study area is constant. By using the energy balance equation (*Equation 6)*, the instantaneous evapotranspiration as the residual energy balance can be defined.

5.3. HYDRUS 1D simulation

5.3.1. Pre-processing of simulation

The model used in this study simulates one-dimensional water flow in a typically bare soil condition. Simulations were performed for 2 periods of 2 different years; 2009 and 2010. For 2009, simulation was performed for the period of August 7th - October 1st. In 2010, it was performed for the period of June 25th - September 10th. These simulation periods was based more on the completeness of precipitation and meteorological data as time-variable boundary condition of the model. The simulation was carried out with hourly temporal resolution.

The profiles of each soil are varying, from a 10 cm to 275 cm in depth and from 1 layer soil profile to 7 layers. The soil surface boundary condition included actual precipitation during the time of simulation. The bottom boundary condition was set as free drainage. This type of boundary condition is used for the situation where the water table lies far below the domain of interest.

5.3.2. Soil hydraulic property model

Six types of models for the soil hydraulic properties are provided in the code of HYDRUS 1D. The van Genuchten-Mualem (Van Genuchten, 1980) was selected for the hydraulic model. The hydraulic model was based on the following governing equations:

$$\theta(h) = \begin{cases} \theta_r + \frac{\theta_s - \theta_r}{[1+|\alpha h|^n]^m} & h < 0 \qquad \text{Equation 47} \\ \theta_s & h \geq 0 \qquad \text{Equation 48} \end{cases}$$

$$K(h) = K_s S_e{}^1 \left[1 - \left(S_e{}^{1/m}\right)^m\right]^2 \qquad \text{Equation 49}$$

Where, h_s is air-entry value [L], θ_s is saturated water content [-], θ_r is residual water content [-], *a, m, n* - empirical parameters [1/L], [-], [-], S_e is effective water content [-], K_s is saturated hydraulic conductivity [L/T], K_r is relative hydraulic conductivity [-], and $K_k(h_k)$ is unsaturated hydraulic conductivity at pressure head *hk* [L/T]

5.3.3. Soil hydraulic properties

The properties of soil for the van Genuchten-Mualem selected model are listed in Table 5-1.

Table 5-1: Soil hydraulic properties for van Genuchten hydraulic model

Notation	Soil hydraulic properties
θ_r	Residual soil water content
θ_s	Saturated soil water content
Alpha	Parameter *a* in the soil water retention function
n	Parameter *n* in the soil water retention function
K_s	Saturated hydraulic conductivity
l	Tortuosity parameter in the conductivity function

Soil hydraulic properties have been conducted to retrieve the soil hydraulic properties from collected soil samples. Permeameter analysis (constant head and falling head) were conducted to get the saturated hydraulic conductivity, WP4 method was used for determination of the residual moisture content. The soil particle size of soil was determined from texture size analysis.

Using *Rosetta Lite v 1.1* model, where the percentage of particle size is used as input, all the soil hydraulic properties for the van Genucten hydraulic model can be obtained. Rosetta model is a Windows-based program which can estimate unsaturated hydraulic properties from surrogate soil data such as soil texture data and bulk density. Rosetta model use *pedotransfer functions* (PTFs) where the model can translate basic soil data into hydraulic properties (Schaap et al., 2001).

5.3.4. Model calibration

The dataset of soil moisture was used for calibrating soil hydraulic properties to simulate the model. In the previous work, three soil profiles were selected for soil moisture measurement in the study area using hydraprobe sensors at four depths: 25, 50, 75 and 100 cm. The equipment was installed in June 2009. In this study, the model was not calibrated, but all parameters were obtained from measurement.

Balugani et al (2011) had performed the model calibration using soil moisture data. It is stated that the HYDRUS 1D simulation of the soil moisture changes in August-September 2009 is in agreement with the dataset of soil moisture measurement. It is also stated that evaporation rate resulted from the initial soil hydraulic properties and the calibrated ones using soil moisture data have similar values.

5.3.5. Integration with transpiration map

Daily evaporation rates is one of the output variables of HYDRUS 1D. To obtain the rates of daily evapotranspiration, integration with transpiration rates is required. Leonardo Reyes in his PhD research work calculated the transpiration map in the whole Sardon Catchment, up-scaled from sap-flow measurement method.

The transpiration map is a raster image, with resolution of 100x100 m for pixel. Therefore, it is assumed that the value of transpiration rate in the point measurement is the value of the transpiration rate of the pixel. Another assumption is that the transpiration rate of the map does not change over time for the entire season of 2009 and 2010.

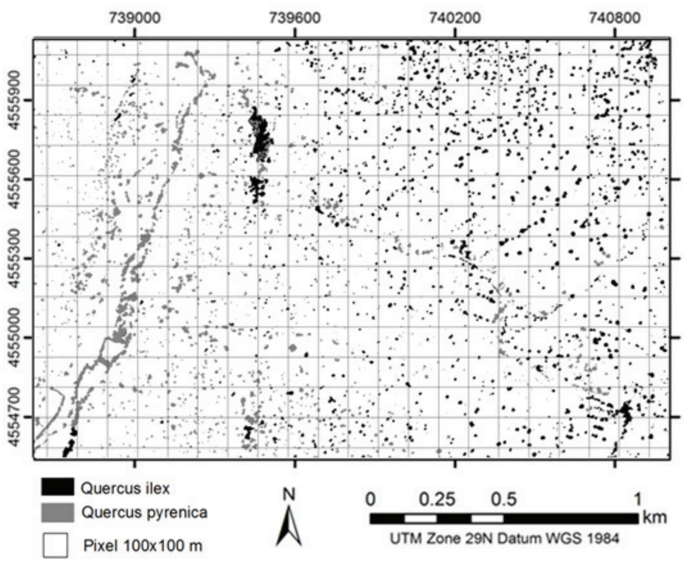

Figure 5-3: Class tree and pixel resolution of transpiration map

5.4. Eddy covariance and flux footprint

The eddy covariance calculation results used in this study were based on calculation method performed by Rwasoka(2010) in his *MSc* research. In *Chapter 4*, the instruments have been presented installed in the Eddy Tower which was able to measure a number of variables. Some variables; turbulent heat fluxes, friction velocity, mean wind speed, sonic temperature and wind variances were determined by an eddy covariance processing software called AltEddy (version 3.5) which was developed by ALTERRA, Wageningen University, The Netherlands. Data processing was performed at 30 minutes intervals.

Actual evapotranspiration can be determined from the measured latent heat flux as the function of air temperature (T_a) as the following equation:

$$\lambda = 2.501 - 2.361x10^{-3}T_a \qquad \textit{Equation 50}$$

Where λ is the latent heat flux (J kg^{-1}) and T_a is the air temperature (^{0}C). Actual evapotranspiration than was calculated by *Equation 51*.

$$ET = \left(\frac{\lambda E}{\lambda}\right) \qquad \textit{Equation 51}$$

The total *ET* is the total evapotranspiration. Total *ET* of 30 minute intervals of flux can be determined by multiplied by 1800 seconds.

From all the data retrieved by eddy tower, potential evapotranspiration (PET) was also calculated. Two difference algorithm approaches were used to obtain PET, namely Penmann-Monteith and Priestley-Taylor method. The equation of the two methods was explained in *chapter 2*, page 8 *(Equation 30 – Equation 32)*.

The eddy flux footprint was also based on the model determination used by Rwasoka (2010). The footprint model has been developed by Hsieh et al (2000) and Detto et al. (2006). In this model, the footprint was related with measurement height, surface roughness and the atmospheric stability.

5.5. Result comparison

The main objective of this study is to compare two approaches; remote sensing approach and hydrological model simulation approach, for the estimation of evapotranspiration in dry climate area, and validate them using the evapotranspiration result of the eddy covariance method. Therefore, result comparison and evaluation is the main content of this study.

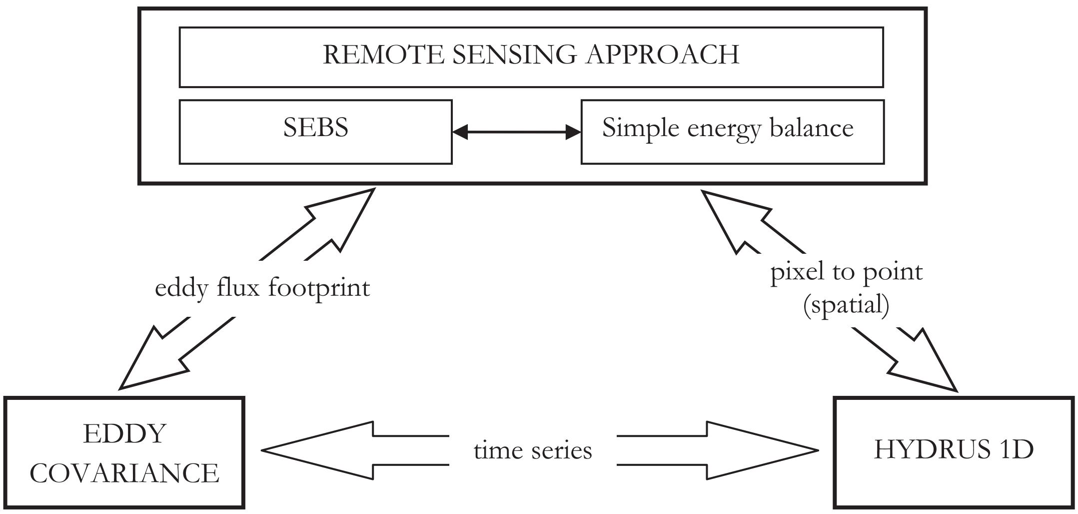

Figure 5-4: General flowchart in evapotranspiration result comparison

The different approaches should be applied for comparing each method against another in order to obtain the reliable comparison result which was more based on the output of each approach. Figure 5-4 shows the general depiction in comparing the three result of method used in this study.

5.5.1. Comparison AET of remote sensing approach and HYDRUS 1D

The daily evapotranspiration calculated by remote sensing approach is in the form of map which contains the value in each pixel. Each pixel is 30x30 m in spatial resolution. This is quite different from HYDRUS 1D. An AET of HYDRUS 1D is a point value which is resulted from point measurement and simulation. There are 17 points of HYDRUS 1D AET which are distributed in the study area.

It is assumed that the point simulated is representative of the whole 30x30 m pixel in which is included (Figure 5-5).

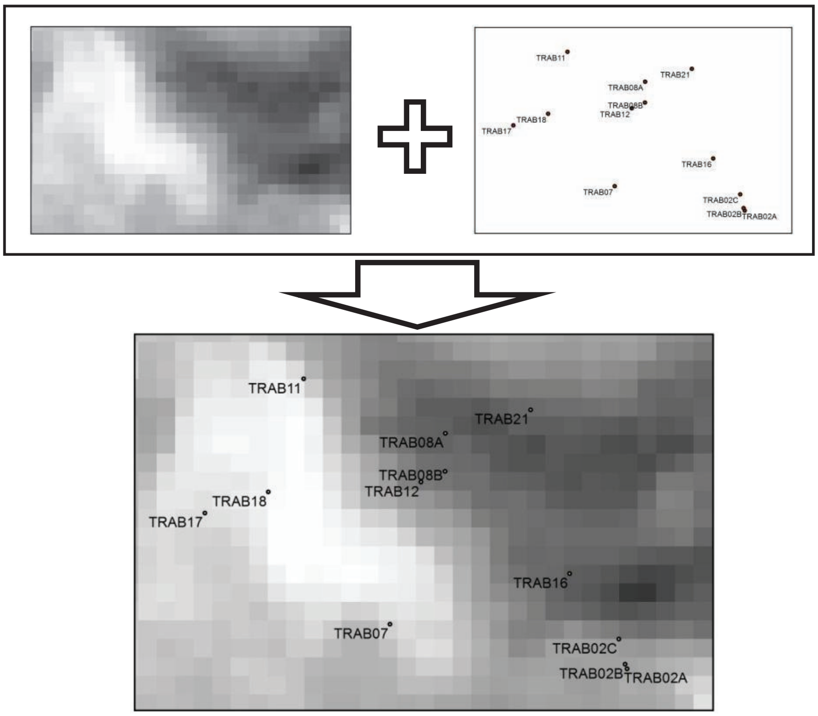

Figure 5-5: Illustration showing the comparison between pixel and point

5.5.2. Comparing AET of remote sensing approach with eddy covariance

The comparison of AET (or other fluxes) resulted by remote sensing approach with eddy covariance can be performed by applying the relative contributions of footprint area as a weighting function to the pixels concerned.

The spatial resolution of footprint area is 1x1 meter, while the pixel resolution of the images (flux) resulted from LANDSAT is 30x30 meter. To apply the weighting function, it needs the same spatial resolution of the two images; the area of footprint and the area of the image. Therefore, a resampling method is needed. In order to obtain the weighing of each different contribution of footprint area, the images were resampled into the footprint resolution, which is 1x1 meter.

For comparison, the weighted average flux within the footprint area can be determined by using the following function (van der Kwast et al., 2009) :

$$\hat{\mu} = \sum_{I=1}^{N} W_i X_i \qquad \textit{Equation 52}$$

Where, X_i is the flux (of remote sensing approach) at pixel i, W_i is the relative contribution of footprint area and N is the number of pixels in the footprint. The sum of the weights should equal to 1. The footprint weighted variance of the fluxes is then calculated by:

$$\hat{\sigma}^2 = \left(\frac{\sum_{i=1}^{N} W_i}{\left(\sum_{i=1}^{N} W_i\right)^2 - \sum_{i=1}^{N} (W_i)^2} \cdot \sum_{i=1}^{N} W_i (X_i - \hat{\mu})^2\right) \cdot N^{-1} \qquad \textit{Equation 53}$$

5.5.3. Comparing AET of HYDRUS 1D with eddy covariance

Both output method; HYDRUS 1D and eddy covariance produced time series data of AET. The purpose of the comparison between the two results is to understand the trend of AET fluctuation in 2009 and 2010, especially in dry season.

The processing steps of the comparison are:

1. Selected points of HYDRUS 1D in the footprint area. Three point measurements which are in the footprint area in each year were selected.
2. Plotted the daily AET of HYDRUS 1D versus time.
3. Plotted the daily AET of The eddy covariance versus time
4. Visual inspection of the daily AET versus Julian day.

6. RESULTS AND DISCUSSION

6.1. Remote sensing approach

6.1.1. Land surface temperature (LST) and Vegetation Index (NDVI)

Besides having direct relationship with sensible and latent heat exchange processes, land surface temperature is greatly influenced by land use and land cover. Land surface temperatures of the study area in four different dates was calculated based on image processing from thermal band of LANDSAT 5 TM (Figure 6-1)

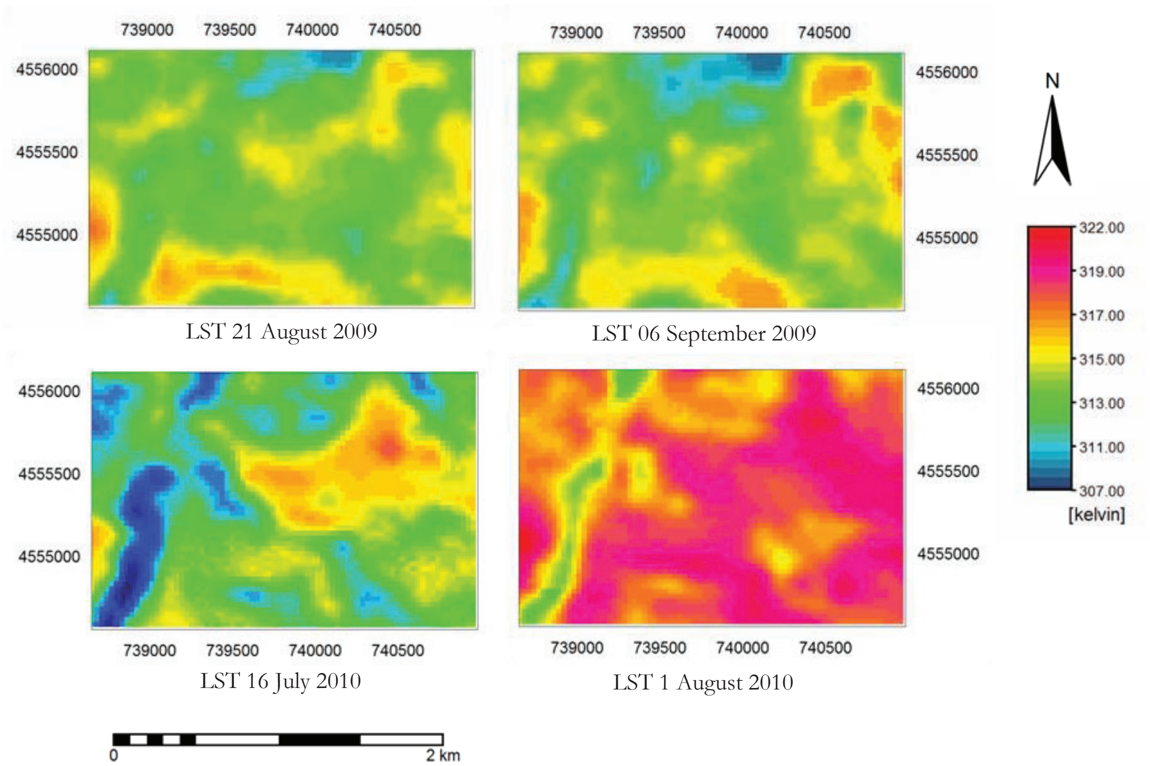

Figure 6-1: The maps showing Land Surface Temperature (LST) in the different dates

The values of LST in four dates are quite similar, ranging from 307.1 to 322.4 Kelvin. LST of August 1, 2010 has the highest value (312.4 – 322.4 K).

The difference between land surface temperature and air temperature (LST-T_a) is a main parameter in calculating sensible heat (H) in simple energy balance equation. Therefore, air temperature in the time of LANDSAT overpass (T_a) is also an important factor. T_a is obtained from the tower station in each date which is constant for the whole area. It is obvious in Figure 6-1, that the (LST-T_a) of August 1st 2010 has the lowest value although the LST of this date showing the highest values of all four dates. This was caused by the high value of air temperature at this time (Table 4-3).

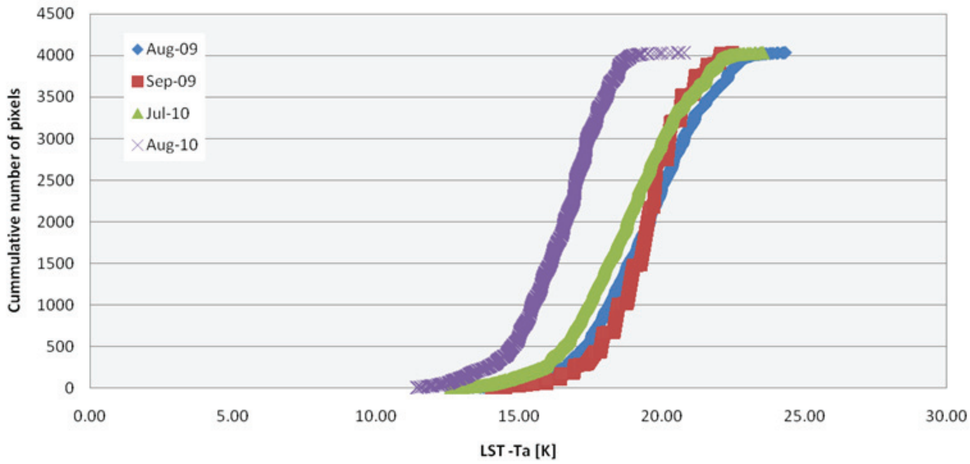

Figure 6-2: Graphic showing the value of (LST-T_a)

In SEBS, NDVI is an important input map, especially if there is no sufficient information about land use in the area. NDVI is used to obtain the Leaf Area Index (LAI) and fractional cover (f_c) map.

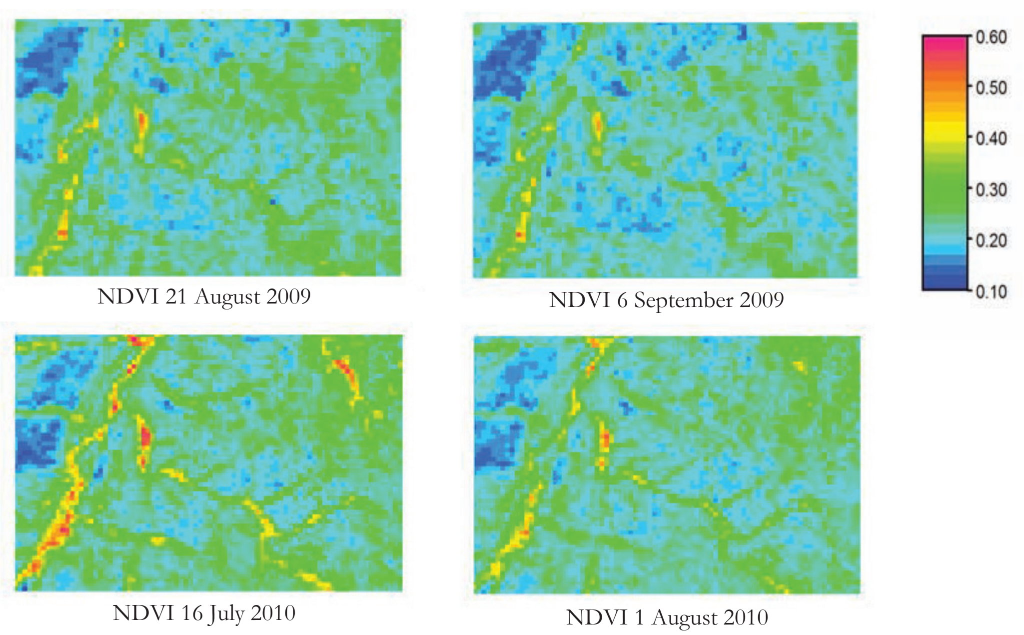

Figure 6-3: NDVI maps in the study area,
the scale, north direction and coordinates of maps correspond with Figure 6.1

As shown in Figure 6-3, NDVI map of all dates have similar values ranging from 0.10 - 0.60. This is a result of the fact that the images are calculated in dry season. The higher values of NDVI observed in the area correspond to the stream, where the tree density is higher than in the rest of the area.

6.1.2. Sensible heat flux

In the surface energy balance, sensible heat flux (*H*) becomes the most important flux, because of its complexity calculation especially for SEBS algorithm, which is explained in the previous chapter. The difference approaches used to calculate *H* in SEBS and in the simple energy balance resulted in the different of sensible heat flux values.

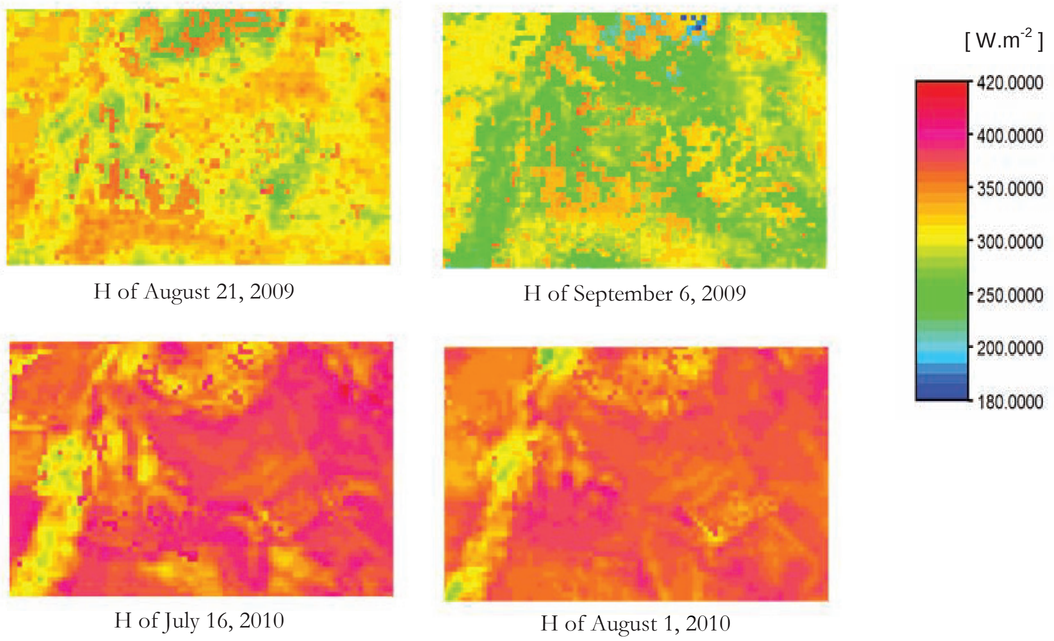

Figure 6-4: Sensible heat flux resulted from SEBS algorithm,
the scale, north direction and coordinate of maps correspond with Figure 6.1

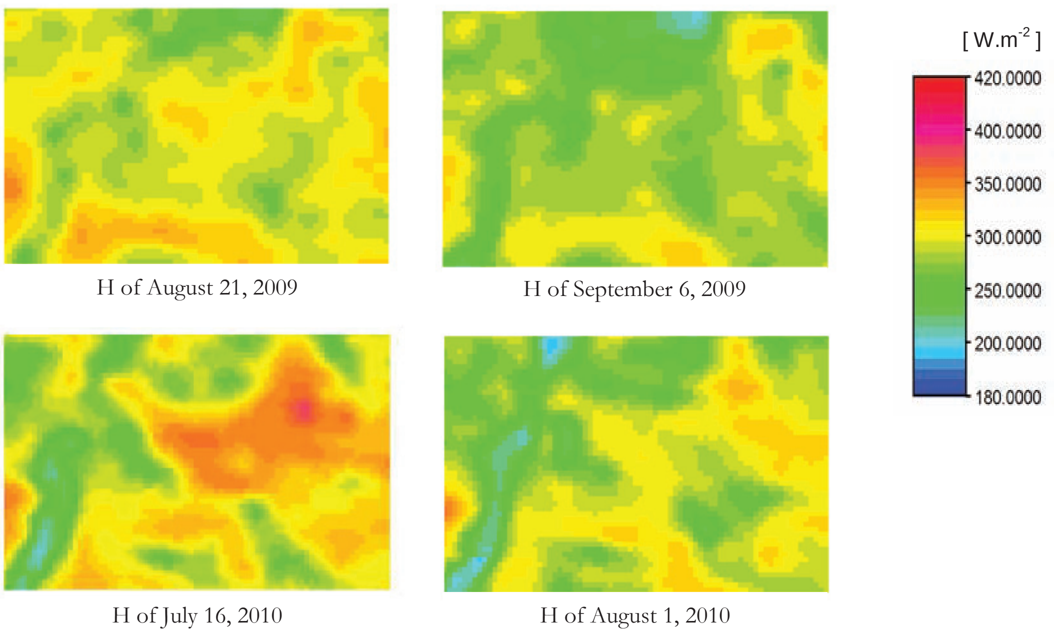

Figure 6-5: Sensible heat flux resulted from the simple energy balance,
the scale, north direction and coordinate of maps correspond with Figure 6.1

In the simple energy balance calculation, sensible heat flux is a function of (LST-*Ta*) and the aerodynamic resistance. By assuming that the aerodynamic resistance in this area is homogeneous, the sensible heat flux is only influenced by the value of LST-*Ta*. Instead, the calculation *H* in SEBS considers many parameters, including wind speed and land use map which was derived from the NDVI map.

In the SEBS result, *H* of 2009 and 2010 show very different values while *H* in 2010 has very high values. It is mainly caused by the value of wind speed which the wind speed of 2010 is much higher than in 2009 (Table 4-3). High wind speed causes a lower aerodynamic resistance (*Equation 11),* and thus a higher *H*

(Equation 7). In 2009, H values range from 202.18 to 383.53 W.m^{-2} in August and 184.27 – 360.34 W.m^{-2} in September. In 2010, H values vary from 277.89 to 415.73 W.m^{-2} in July and 257.43-404.89 W.m^{-2} in August. While H calculated from the simple energy balance is more homogeneous in all four different dates, it ranges from 195.15 to 379.53 W.m^{-2}.

6.1.3. Daily actual evapotranspiration (AET)

Instantaneous latent heat flux (λE) was obtained after all the individual maps of net radiation (R_n), sensible heat flux (H) and soil heat flux (G) were evaluated. From λE, the daily evapotranspiration (AET) was derived by *Equation 19,* as the function of daily evaporative fraction (Λ).

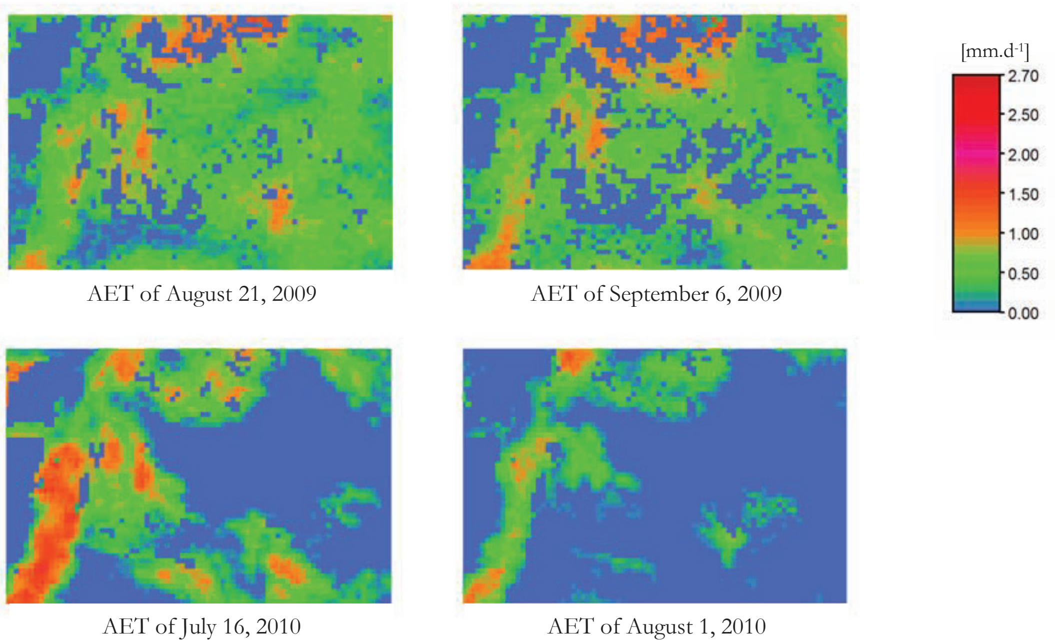

Figure 6-6: Actual evapotranspiration resulted from SEBS algorithm,
the scale, north direction and coordinate of map correspond with Figure 6.1

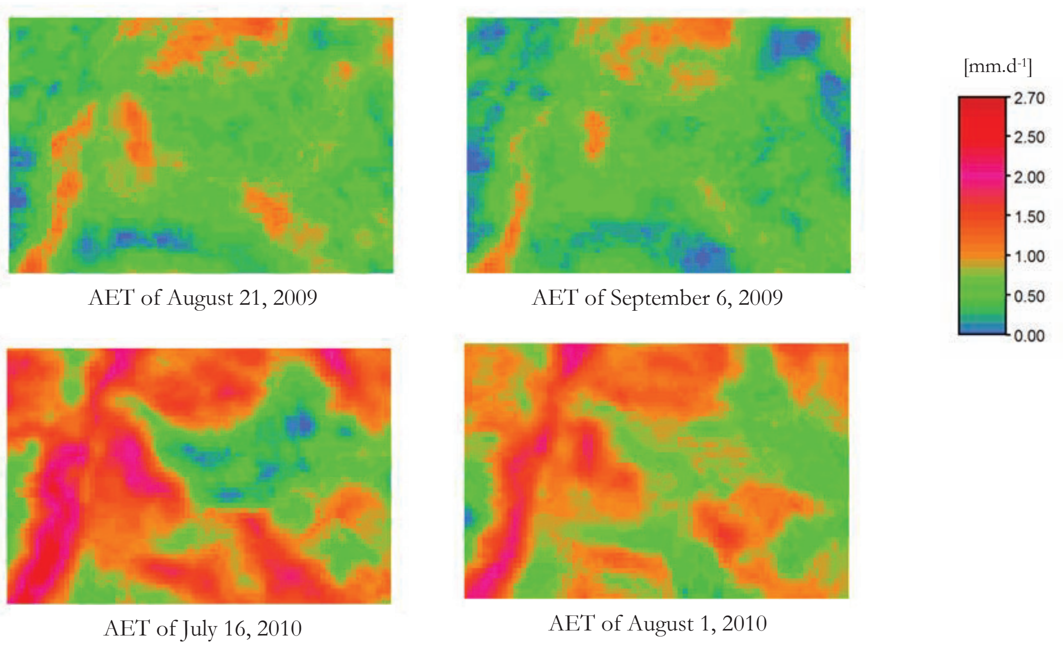

Figure 6-7: Actual evapotranspiration resulted from the simple energy balance
the scale, north direction and coordinate of map correspond with Figure 6.1

In Figure 6-6 and Figure 6-7, it is obviously shown that the values of AET of two different remote sensing approaches are in different pattern, especially in 2010. As explained before, this difference is caused mainly by the different approach in calculating *H*. The general statistic of AET values in the study area is presented in Table 6-1.

Table 6-1: The general statistic of AET values in the study area estimated by remote sensing approach

Date		AET value [mm.d^{-1}]					
		SEBS			The simple energy balance		
		minimum	maximum	average	minimum	maximum	average
2009	August-12	0.000	1.460	0.423	0.000	1.400	0.594
	September-12	0.000	1.420	0.405	0.000	1.300	0.497
2010	July-12	0.000	1.700	0.310	0.000	2.610	1.096
	August-12	0.000	1.350	0.115	0.000	2.120	0.960

In 2009, the values of AET have the same trend, except the low values (≈0) which are produced by SEBS (Figure 6-8). These 0 values of AET are all found in pixels with very low values of NDVI (< 0.2) in these dates (Figure 6-9). In 2010, the AET value of SEBS is much lower than the simple energy balance as previously explained due to the high wind speed in these dates which made the value of SEBS *H* much higher.

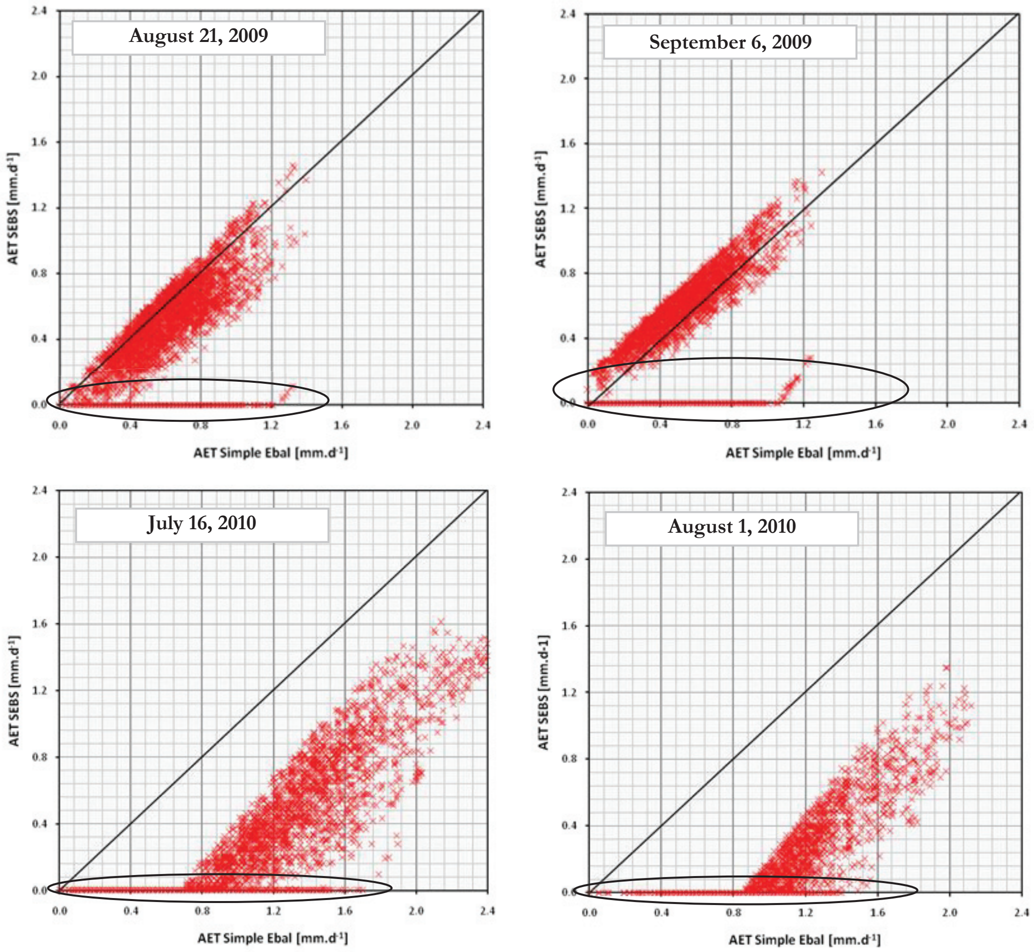

Figure 6-8: Actual daily evapotranspiration (AET) of SEBS versus AET of Simple energy balance

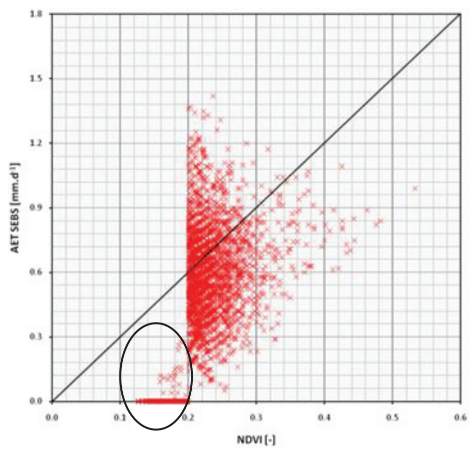

Figure 6-9: Actual daily evapotranspiration (AET) of SEBS versus NDVI of September 6, 2009

6.2. HYDRUS 1D simulation

6.2.1. Soil hydraulic properties

For comparison, the saturated hydraulic conductivities resulted from five samples analysed with permeameter were compared with the saturated hydraulic conductivity from the *Rosetta* model. Although not in 1:1 line, the correlation of the two results is in agreement (Figure 6-10). It means that soil hydraulic properties resulted from *Rosetta* model simulation has the values that can be used as input in HYDRUS 1D.

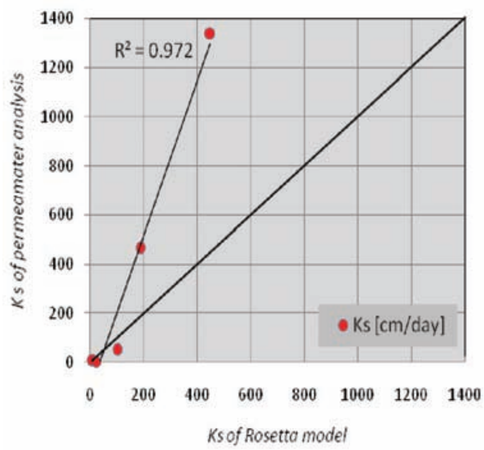

Figure 6-10: Saturated hydraulic conductivity from two different approaches

According to United States Department of Agriculture (USDA) classification (Soil Survey Division Staff, 1993), the class of the soil in the study area is range from *sand* to *sandy loam* (Figure 6-11).

Therefore, based on the USDA classification, the soil in the study area is quite homogeneous, which is *sandy soil*. According to the description of soil texture during field work, the soil texture has the similar characteristic over the whole area. In vertical profile, the soil texture displayed heterogeneity, especially for deeper soil depth (e.g. TRAB 06). It was typically finer in the first centimetres with higher percentage of fine sediments in the upper profile and presence of gravel in the deeper part of the soil, and then slowly turning into fractured granite at the bottom of the soil profile (Figure 6-14).

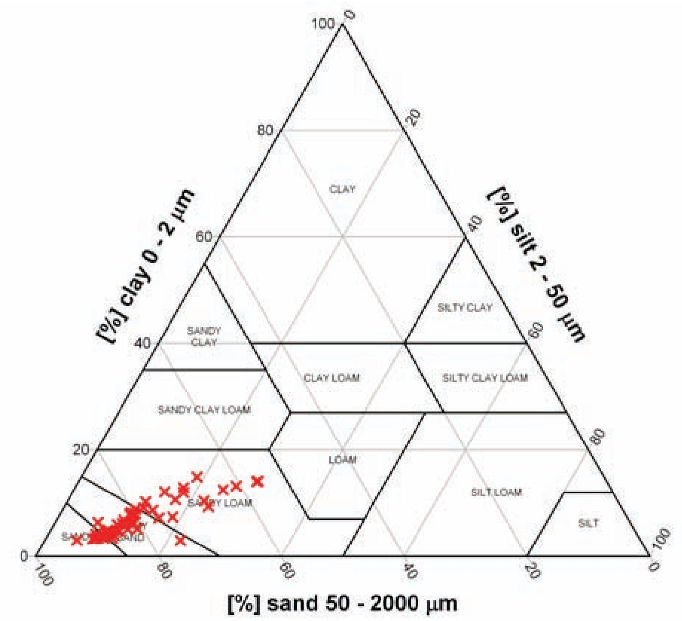

Figure 6-11: USDA classification for soil texture class

The descriptive statistic of soil properties was conducted to describe of the heterogeneity of the soil property in the study area (see Figure 6-12 and Figure 6-13). However, from the descriptive analysis is evident that the soil texture in the study area is quiet homogeneous.

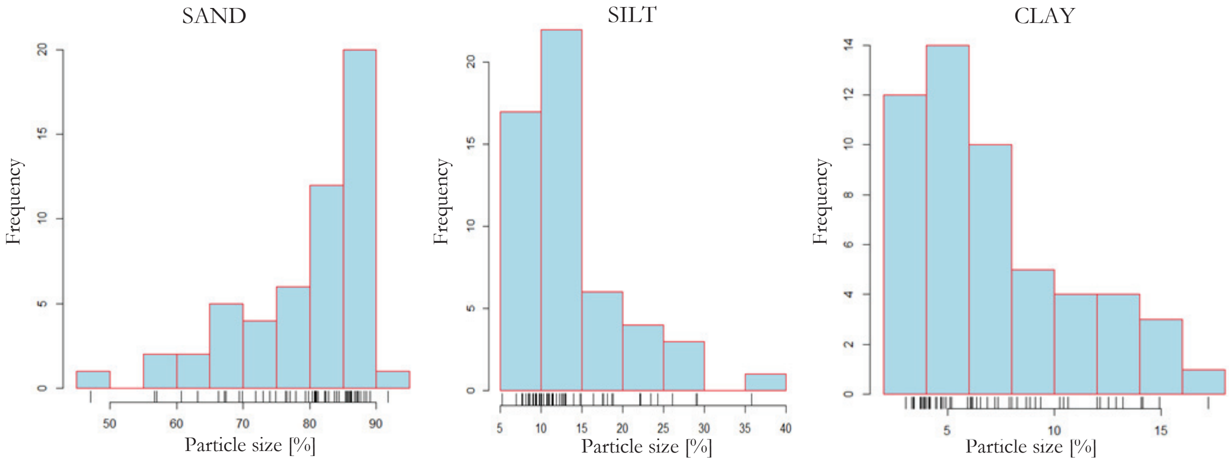

Figure 6-12: Histogram of soil particle size

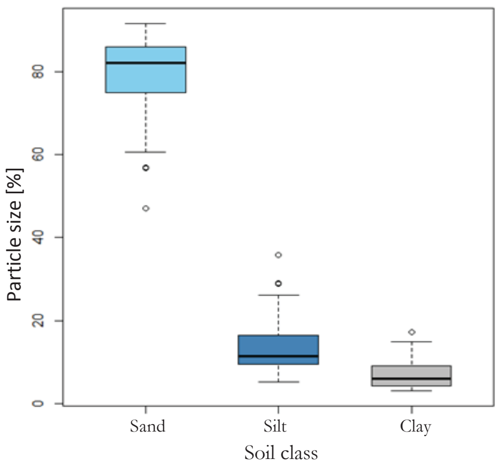

Figure 6-13: Box plot of soil particle

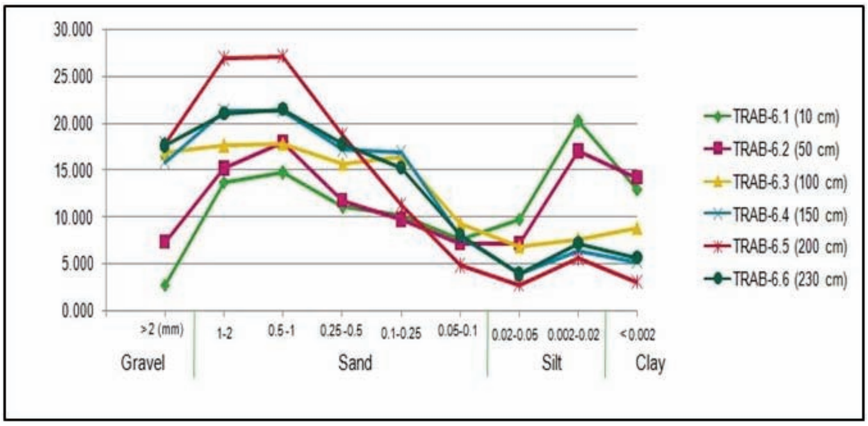

Figure 6-14: The percentage of particle size in TRAB 06

6.2.2. Time series of daily evapotranspiration

A number of output variables resulted from the HYDRUS 1D simulation. One of them is the time series of actual surface flux which contains daily rate of evaporation and infiltration. Evaporation shows as positive value and the rate of infiltration for negative value.

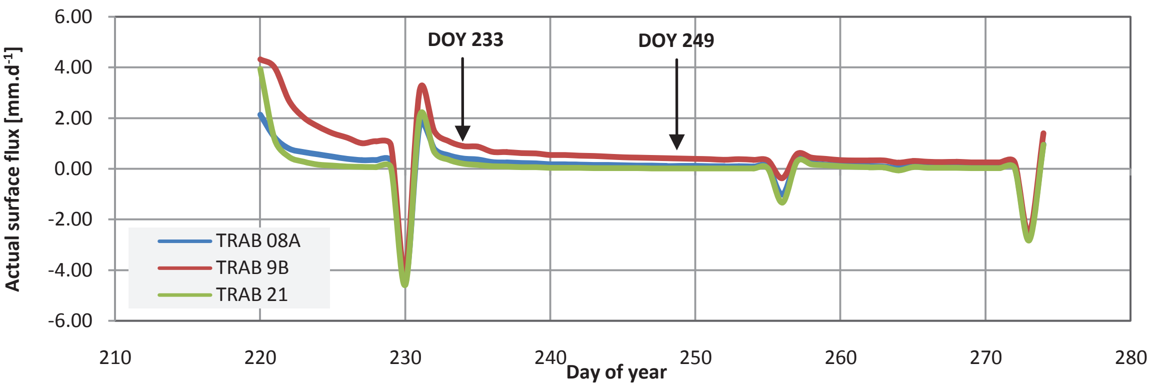

Figure 6-15: Time series daily evaporation of 2009 from HYDRUS 1D and LANDSAT overpass

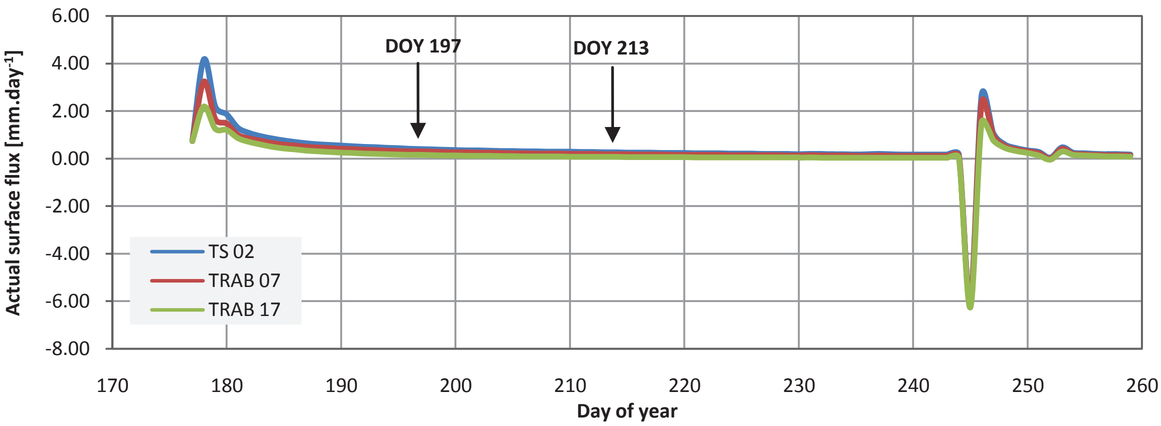

Figure 6-16: Time series daily evaporation of 2010 from HYDRUS 1D and LANDSAT overpass

In the previous chapter is explained that due to the data availability, the model was simulated in two different years separately; 2009 and 2010. In each year, 17 locations have been simulated and resulted data of actual surface flux which contains data of evaporation rate.

Each graph in Figure 6-15 and Figure 6-16 shows the time series data of actual surface flux in 3 different locations. By considering the area which is situated near the eddy tower and the footprint area, these locations were selected in order to compare with time series actual daily evapotranspiration of eddy covariance.

Figure 6-15 and Figure 6-16 also show the time of LANDSAT overpass which will be compared subsequently with the result of remote sensing approach. Daily evaporation of each location in the time of LANDSAT overpass is shown in Table 6-2 and then compared to daily actual evapotranspiration after transpiration was added.

Table 6-2: Daily evaporation in each location in 2009 and 2010

No	Location	Daily evaporation [mm.d^{-1}]				Information in the corresponding pixel
		2009		2010		
		DOY 233	DOY 197	DOY 213	DOY 249	
1	TRAB-02C	0.241	0.127	0.068	0.047	2 small trees, no outcrop.
2	TRAB-03	0.322	0.070	0.033	0.065	1 tree, no outcrop
3	TRAB-04	0.371	0.092	0.043	0.083	1 tree, no outcrop
4	TRAB-05	0.431	0.162	0.093	0.127	no tree, 2% outcrop
5	TRAB-06	1.067	0.655	0.431	0.518	the stream area, 1 small tress, no outcrop.
6	TRAB-07	0.582	0.290	0.187	0.233	no tree, ~2% outcrop
7	TRAB-08A	0.406	0.132	0.073	0.110	1 tree, no outcrop
8	TRAB-09A	0.701	0.377	0.240	0.289	the stream area, 2 trees, no outcrop
9	TRAB-09B	0.939	0.444	0.291	0.420	the stream area, 2 trees, no outcrop
10	TRAB-12	0.894	0.408	0.260	0.393	no tree, no outcrop
11	TRAB-13	0.344	0.057	0.027	0.044	1 small tree, no outcrop
12	TRAB-14	0.737	0.297	0.173	0.262	2 trees, no outcrop
13	TRAB-15	0.351	0.207	0.107	0.067	1 tree, no outcrop
14	TRAB-17	0.461	0.147	0.073	0.115	2 trees, no outcrop
15	TRAB-21	0.205	0.162	0.085	0.014	1 small tree, no outcrop
16	TS2	0.843	0.388	0.265	0.382	no tree, no outcrop
17	TB05B1	0.187	0.020	0.009	0.014	1 tree, no outcrop

Table 6-3: Transpiration rate in each location of the study area

Location	T [mm.d^{-1}]	Location	T [mm.d^{-1}]
TRAB-02C	0.023	TRAB-12	0.008
TRAB-03	0.065	TRAB-13	0.007
TRAB-04	0.015	TRAB-14	0.030
TRAB-05	0.005	TRAB-15	0.018
TRAB-06	0.029	TRAB-17	0.017
TRAB-07	0.025	TRAB-21	0.035
TRAB-08A	0.008	TS2	0.028
TRAB-09A	0.050	TB05B1	0.039
TRAB-09B	0.050		

The transpiration rate in Sardon catchment area is very low, as expected for a typical open woodland area. Transpiration rate in the footprint area in the study area is only 7.2 % from total evapotranspiration Balugani et al (2011). Table 6-3 shows the value of transpiration rate in the pixel with each point measurement inside.

6.3. Eddy covariance and flux footprint

6.3.1. Eddy covariance evapotranspiration

Potential and daily evapotranspiration were calculated from the eddy tower measurement variables. As explained in the previous chapter, two different methods were used in calculating potential evapotranspiration; Penmann-Monteith (PM) and Priestley-Taylor (PT). The time series of evapotranspiration value in the year 2009 and 2010 are presented in Figure 6-17 and Figure 6-18.

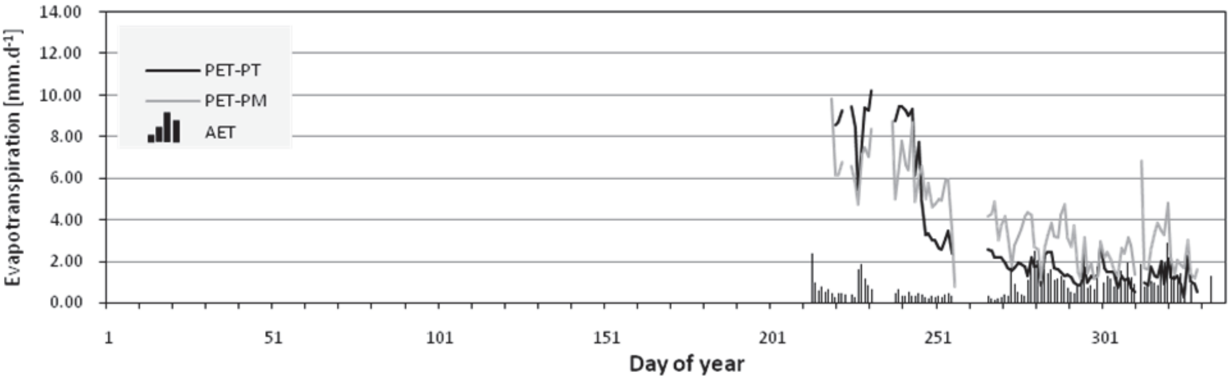

Figure 6-17: Potential and actual evapotranspiration in 2009 from eddy covariance method

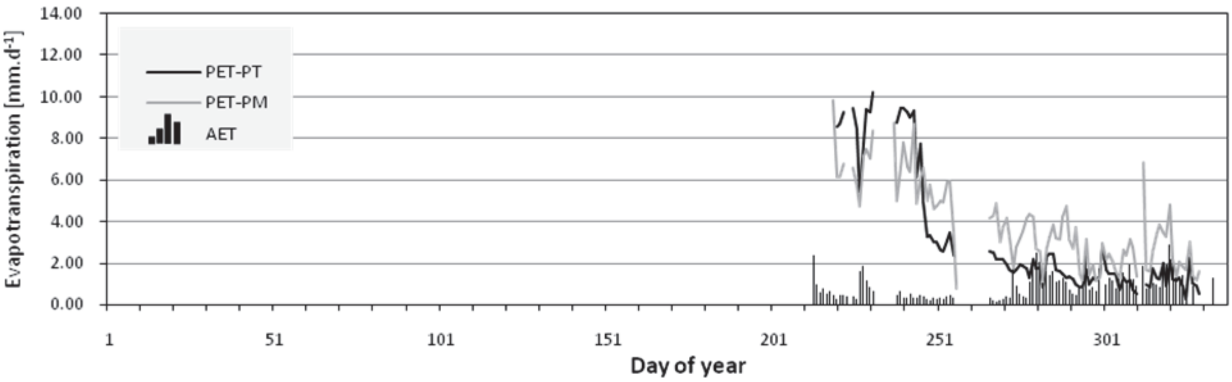

Figure 6-18: Potential and actual evapotranspiration in 2009 from eddy covariance method

Generally, potential *ET* resulted from Prestley (PT) is lower than Penmann-Monteith (PM) in dry season and more equal in wet season with adequate rainfall events. As explained in the previous chapter that PT equation is a simplification of PM equation by reducing data requirement which is only ideal for wet surface condition with no advection. Penmann-Monteith equation cannot be used for the calculation of potential *ET* when the surface is dry and consequently, the air above is also dry (Brutsaert & Stricker, 1979).

6.3.2. Eddy flux footprint

There are two days eddy flux footprint processed due to the data availability, namely: September 16, 2009 and July 16, 2009. In comparing with evapotranspiration resulted from remote sensing approach, the time of eddy flux footprint must be same with LANDSAT overpass time, which is at 13.00 local time (GMT +2).

The two footprints show the different contribution area (Figure 6-19). The different tone of blue color represents the different probability of contribution. The closer the area to the tower, the higher the value of the contribution probability. In September 16, 2009, the footprint area is in North-East of the eddy tower, while in July 16, 2010, the footprint area is in South-West of the eddy tower.

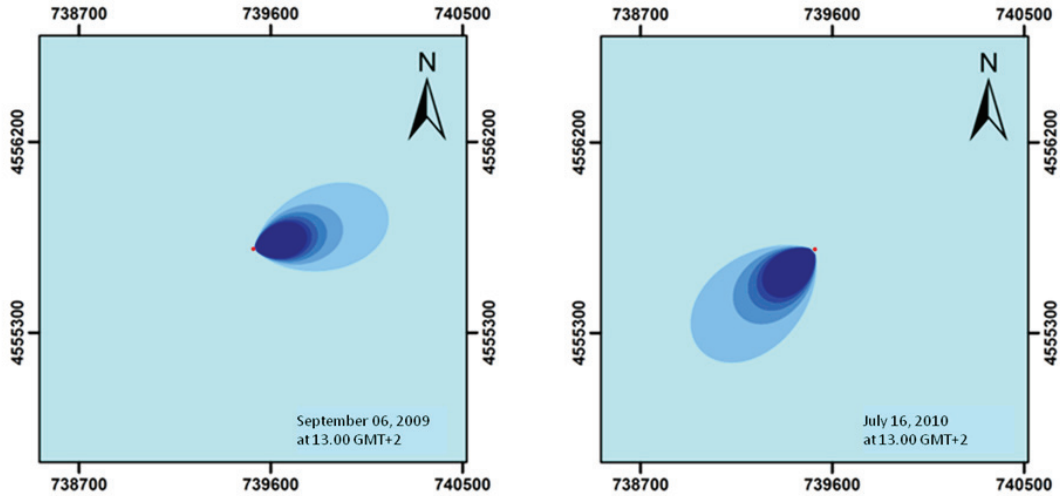

Figure 6-19: The eddy flux footprint in two different dates

6.4. Comparison AET of remote sensing approach and HYDRUS 1D

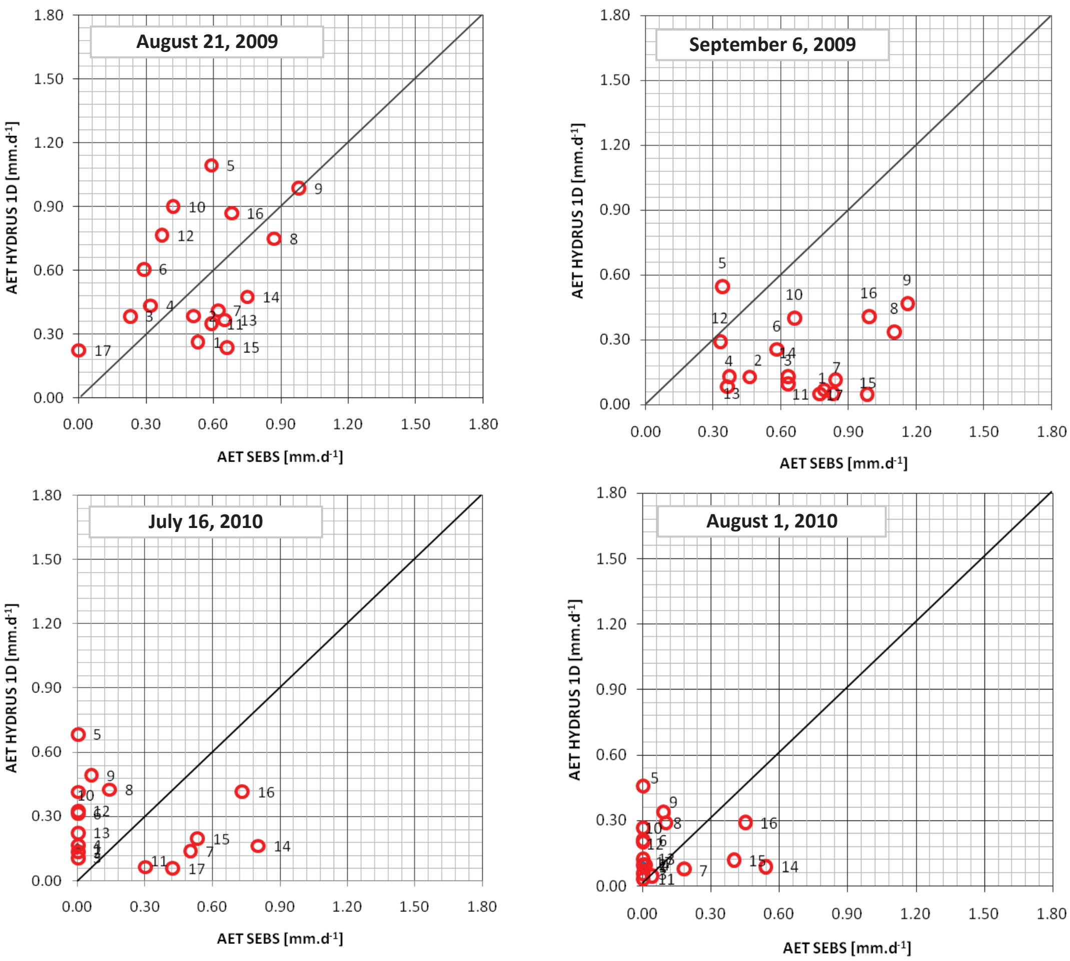

Figure 6-20: AET of SEBS versus AET of HYDRUS 1D

Generally, AET value resulted from remote sensing approach is higher than AET of HYDRUS 1D which are shown in Figure 6-20 and Figure 6-21.

In 2009 (the upper two graphs in Figure 6-20 and Figure 6-21), due to the similar values of AET calculated by two RS approaches, the graphs show similiar relationship between AET of RS and HYDRUS 1D. In this year, there are some values from AET of RS which are higher than AET of HYDRUS 1D, especially in August. Although the study is focus on dry season, some low amount of rainfall occurred. This is the reason why the evaporation (AET) resulted from HYDRUS 1D is quite high in August 21 2009; rainfall was occurred in August 19 2009, two days before the satellite overpass.

In addition, in September 2009, there is one point which has high AET value of HYDRUS compared to RS value; it is TRAB 06 (no. 5). TRAB 06 has the deepest soil profile which is 235 cm, and the top layer has more clay soil (> 10%) with lower K_s (< 35 cm.d^{-1}). This is as expected that in fine textured soil (clayey material), the capillary rise of water is slower but covers a long distance.

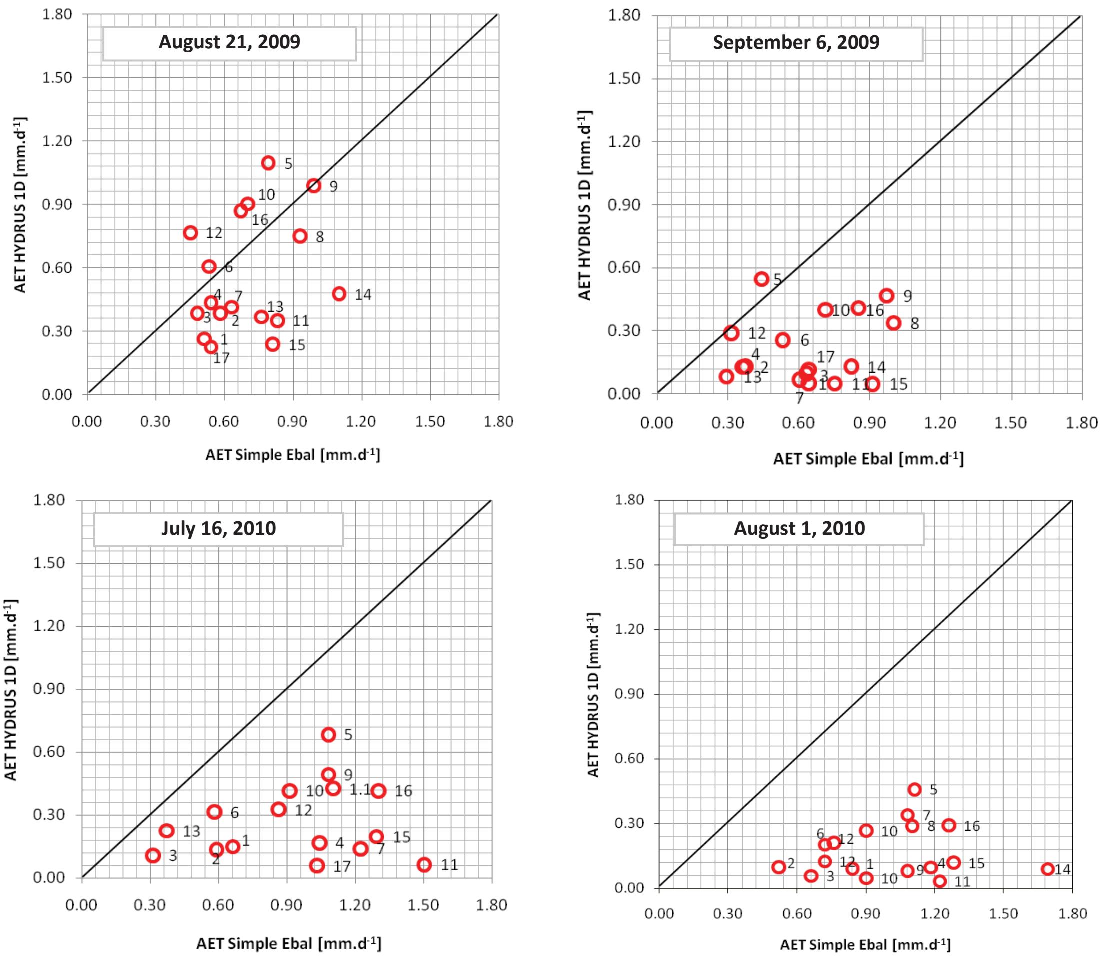

Figure 6-21: AET of Simple energy balance versus AET of HYDRUS 1D

In 2010, the two RS method produced different result of AET. Because of the simplification approach as the previous explanation, the AET values of the simple energy balance are much higher than HYDRUS 1D result. On the other hand, although some AET values of SEBS are also higher then AET of HYDRUS 1D, two points are found which AET values of SEBS are lower than AET of HYDRUS 1D. Also, some 0 values are found in AET of SEBS. However, it can be said that generally HYDRUS 1D given lower value of AET than RS approach.

In addition, 2 (two) points found that AET estimated by HYDRUS 1D have higher values than SEBS are TRAB 09A and TRAB 09B (no. 8 and 9). Those two locations have fairly deep soil profiles (>100 cm) and contain more clay soil in the top soil (>10%) and quite low Ks (40 - 62 cm.d^{-1}). In TRAB 06 (no. 5), the AET value of HYDRUS 1D also the highest value, 0.68 and 0.46 mm.d^{-1}, in July 16 and August 1, 2010, respectively. Because of pixel value (AET) of SEBS shown in TRAB 06 is 0; the comparison cannot be taken into account.

6.5. Comparison AET of remote sensing approach and eddy covariance

As shown in Figure 6-22, the eddy footprints of two dates are positioned in different area (see Figure 6-19). In September 6 2010, it is sited North-East of the eddy tower and has more homogeneous area; bare land with sparse vegetation. On the other hand, the footprint area of July 16 2010 has a more varied land cover. The area has more vegetation, also Sardon and La Mata streams are inside the area.

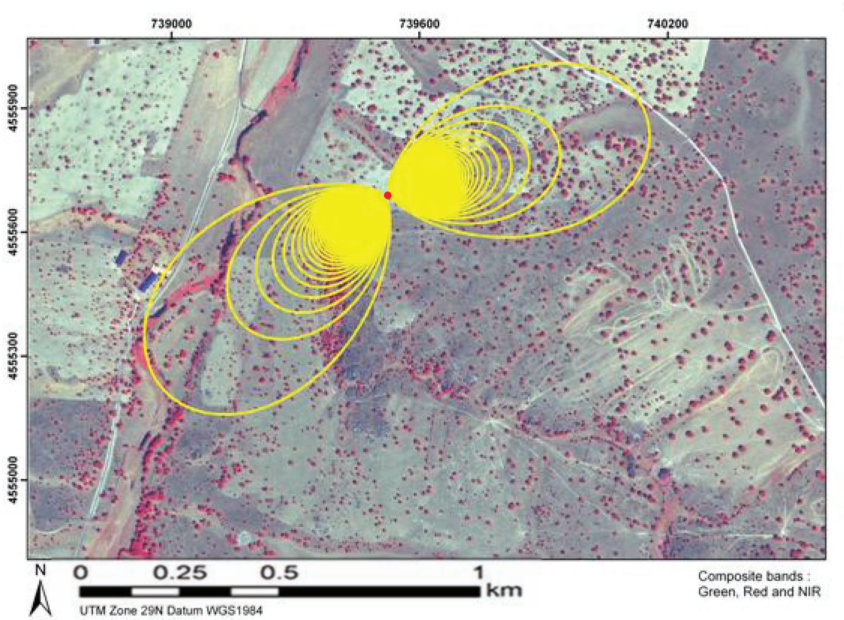

Figure 6-22: Location in the study area with the contribution of eddy flux footprint to the eddy tower

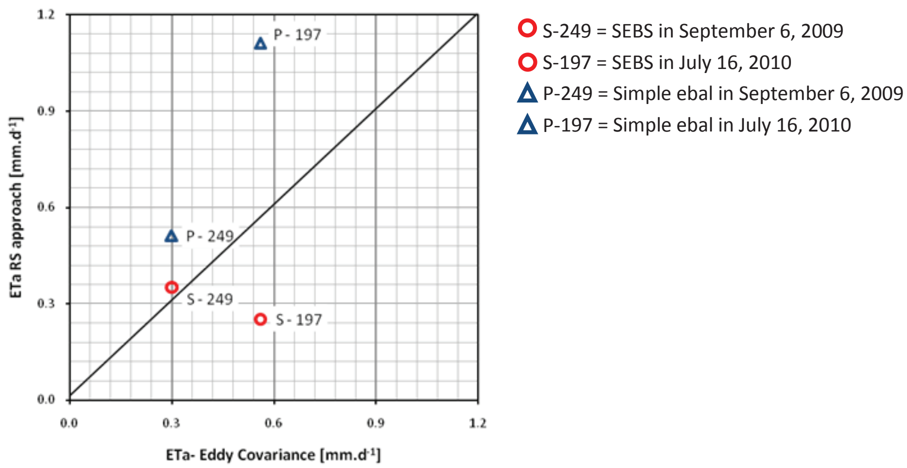

Figure 6-23: Measured AET of eddy covariance method versus remote sensing approach

The simplified equation in *Equation 54* used to express the change in percentage for the relationship estimation, with AET of EC is used as reference AET.

$$X = \frac{(AET_{Rs} - AET_{ref})}{AET_{ref}}$$ *Equation 54*

Table 6-4: Comparison of AET result between RS approaches and Eddy covariance

Date	AET of RS [mm.d^{-1}]		AET of EC [mm.d^{-1}]	X [%]
September 6, 2009	SEBS	0.352	0.299	17.98
	S-ebal	0.512	0.299	71.52
July 16, 2010	SEBS	0.253	0.560	-54.88
	S-ebal	1.111	0.560	98.45

As shown in Table 6-4, it is presented that the outputs of the two approaches are quite different. However, compared to the eddy covariance as AET reference, remote sensing AET in 2009 show the better result. Also, SEBS algorithm produced the better AET output rather than the simple energy balance.

6.6. Comparison AET of HYDRUS 1D and eddy covariance

Figure 6-24 and Figure 6-25 show the comparison of time series AET of HYDRUS 1D and AET of eddy covariance. From the two estimation years, it can be said that HYDRUS 1D estimated the lower value of AET with respect to the eddy covariance method, especially in 2010 which the AET value of eddy covariance is much higher than AET estimated by HYDRUS 1D. The initial drop in HYDRUS AET is due to the initial condition.

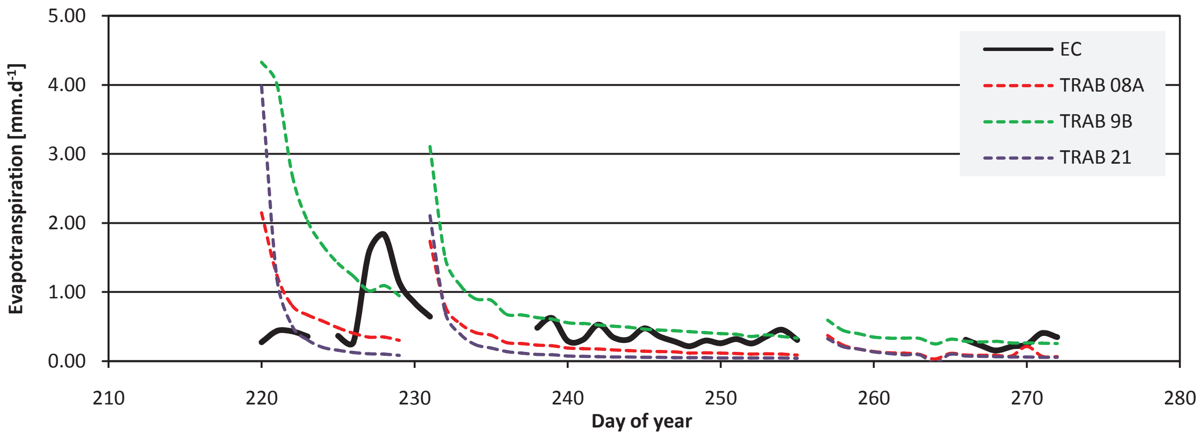

Figure 6-24: Time series showing AET of eddy covariance and AET of HYDRUS 1D in 2009

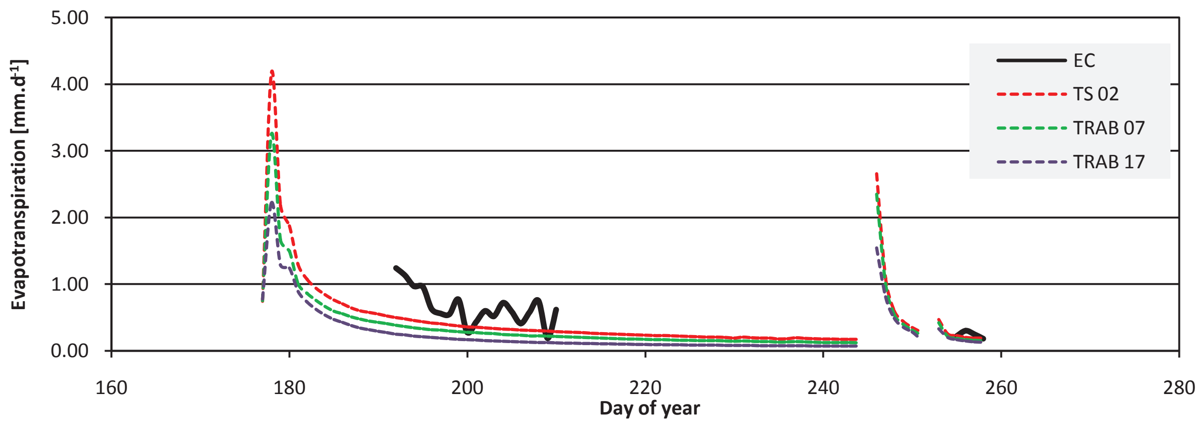

Figure 6-25: Time series showing AET of eddy covariance and AET of HYDRUS 1D in 2010

AET of eddy covariance is more varied, whereas AET of HYDRUS only shows the decreasing flat data with no fluctuation each day. The general statistic of AET values of the two approaches during the dry season is presented in Table 6-5. Due to the difference data availability, the calculation was conducted based on the availability of eddy covariance AET. In 2009, the calculation was performed from August 28 to September 12, while in 2010; it was performed from July 11 to August 5.

Table 6-5: The general statistic of AET values of HYDRUS 1D and eddy covariance method

	AET 2009 [$mm.d^{-1}$]		AET 2010 [$mm.d^{-1}$]	
	HYDRUS 1D	**EC**	**HYDRUS 1D**	**EC**
minimum	0.045	0.217	0.086	0.190
maximum	0.631	0.625	0.383	1.240
average	0.223	0.361	0.192	0.658

7. CONCLUSIONS AND RECOMMENDATIONS

7.1. Conclusions

This study is aimed to compare two approaches in estimating actual evapotranspiration, namely remote sensing (RS) approach and hydrological model simulation approach. The selected study area is located in Sardon-Salamanca; a region in the west of Spain represents the typical semi-arid land area.

In RS approach, two different method were applied, namely SEBS and Simple Energy Balance. As satellite images input, two LANDSAT 5 TM images of 2009 and two of 2010 were used. HYDRUS 1D is the chosen hydrological model was used in this study. By assigning input parameter in pre-processing, like geometry information, soil hydraulic parameter and boundary conditions, the model was simulated and produced a number of post-processing results, including evaporation flux. AET was obtained after transpiration value was added. The eddy covariance method has been used in the study to retrieve direct measurement ET in the study area. This method is a powerful tool that can be used as reference in estimating evapotranspiration.

AET estimated by RS approach which are spatially distributed in the study area can be classified into two results depending on the method used, namely SEBS and the simple energy balance. For SEBS, AET values in the chosen LANDSAT 5 TM images in dry season of 2009 and 2010 vary from 0.00 to 1.70 mm.d^{-1}. Generally, the value of 2009 is higher than 2010 which shown in the average values namely 0.414 and 0.212 mm.d^{-1}, for 2009 and 2010 respectively. For the simple energy balance, AET values in dry season of 2009 and 2010 also show the different ranging values. In 2009, AET values range from 0 to 1.400 mm.d^{-1} with 0.545 mm.d^{-1} as the average value. While in 2010, the values vary from 0 to 2.610 mm.d^{-1} with 0.960 mm.d^{-1} as the average value.

The unsaturated zone model chosen for the ET time series calculation was HYDRUS 1D. Since HYDRUS 1D was used to calculate E component only, T values were later added to calculate ET. The transpiration values used come from the work of Leonardo Reyes (Balugani et al., 2011). In the LANDSAT time overpass, the AET values from HYDRUS 1D range from 0.043 to 1.09 mm.d^{-1} in 2009 and 0.032 – 0.541 mm.d^{-1} in 2010. During dry season and corresponds to the footprint area of eddy covariance, AET values from HYDRUS 1D range from 0.045 to 0.631 mm.d^{-1} in 2009 and 0.086 – 0.383 mm.d^{-1} in 2010.

Generally, AET value estimated from RS approach is higher than AET of HYDRUS 1D. 1n 2009, some values of HYDRUS 1d are higher than AET of RS, especially in August 21 This is related with rainfall event and properties of the soils. In 2010, the remote sensing approach, the simple energy balance, produced very high values of AET and much higher than AET of HYDRUS 1D. This is related to the simplification of the method in calculating sensible heat flux (*H*). However, AET values of two approaches; remote sensing and HYDRUS 1D are not well correlated spatially.

Comparison of the two approaches with the AET retrieving using eddy covariance method as a reference gives the different result. AET estimated from RS approach shows higher values compared with AET of eddy covariance in the eddy tower footprint area, except in July 16, 2010. In general, AET values estimated by HYDRUS 1D are lower than AET from eddy covariance. In 2009, the average AET values during dry season of those two methods; HYDRUS 1D and eddy covariance are slightly similar which are 0.223 mm.d^{-1} for HYDRUS 1D and 0.361 mm.d^{-1} for eddy covariance. In 2010, the AET values of two methods are slightly different. The average AET values of two methods are 0.192 and 0.658 mm.d^{-1} for HYDRUS 1D and eddy covariance respectively.

The comparison result with EC method as reference, HYDRUS 1D gives better agreement than RS approach. HYDRUS 1D also resulted in time series of AET which can be compared to time series AET of EC. But, RS approach is good in giving spatial distribution of AET values which can be compared with EC result in the footprint area. The integration of the two approaches; RS approach and hydrological model simulation, in estimating evapotranspiration in given area can give a better understanding about the availability of evapotranspiration varies , both spatially and temporally.

7.2. Recommendations

1. In regional or local level study of evapotranspiration, the use of LANDSAT 5 TM is good to estimate the spatial variability. However for global monitoring purpose which need the best temporal information available, high temporal resolution image (MODIS/SPOT) is a good choice
2. Ground measurement data are important for hydrological model simulation. With a good density of ground data in the given area, it is possible to calculate reliably the evapotranspiration in the area, and test the reliability of the calculation itself. Time series soil moisture data in each point measurement is important to calibrate the soil hydraulic properties and to simulate the model in each location.
3. The availability of continuous record of micrometeorological data from the eddy tower is essential. As a good reference, eddy covariance will help in validating the flux (including evapotranspiration) estimated from the other methods.
4. With good evapotranspiration data in spatial and temporal, we can easily use the data for various purposes, like groundwater balance calculation, drought monitoring assessment and many more.

LIST OF REFERENCES

Balugani, E., Reyes-Acosta, J. L., Tol, C. v. d., Frances, A. P., & Lubczynski, M. W. (2011). Partitioning and sourcing of dry season evapotranspiration fluxes at the footprint of the eddy covariance in sardon semi-arid location in Spain. *Estudios en la Zona no Saturada del Suelo, X*.

Barsi, J. A., Schott, J. R., Palluconi, F. D., & Hook, S. J. (2005). Validation of a Web-Based Atmospheric Correction Tool for Single Thermal Band Instruments. *Earth Observing Systems X, 5882*.

Bastiaanssen, W. G. M., Menenti, M., Feddes, R. A., & Holtslag, A. A. M. (1998). A remote sensing surface energy balance algorithm for land (SEBAL). 1. Formulation. *Journal of Hydrology, 212-213*, 198-212.

Becker, F., & Li, Z. L. (1990). Towards a local split window method over land surfaces. *International Journal of Remote Sensing, 11*(3), 369-393.

Brutsaert, W. (2005). *Hydrologi, An Introduction*. Cambridge, United Kingdom: Cambridge University Press.

Brutsaert, W., & Stricker, H. (1979). An advection-aridity approach to estimate actual regional evapotranspiration. *Water Resource Research, 15-2*, 443-450.

Detto, M., Montaldo, N., Albertson, J. D., Mancini, M., & Katul, G. (2006). Soil moisture and vegetation controls on evapotranspiration in a heterogeneous Mediterranean ecosystem on Sardinia, Italy. *Water Resour. Res., 42*(8), W08419.

Ding, R., Kang, S., Li, F., Zhang, Y., Tong, L., & Sun, Q. (2010). Evaluating eddy covariance method by large-scale weighing lysimeter in a maize field of northwest China. *Agricultural Water Management, 98*(1), 87-95.

Galleguillos, M., Jacob, F., Prévot, L., French, A., & Lagacherie, P. (2011). Comparison of two temperature differencing methods to estimate daily evapotranspiration over a Mediterranean vineyard watershed from ASTER data. *Remote Sensing of Environment, 115*(6), 1326-1340.

Gieske, A. S. M. (2003). Operational solutions of actual evapotranspiration. 1-14.

Glenn, E. P., Huete, A. R., Nagler, P. L., Hirschboeck, K. K., & Brown, P. (2007). Integrating remote sensing and ground methods to estimate evapotranspiration. *Critical Reviews in Plant Sciences, 26*(3), 139-168.

Gokmen, M., Vekerdy., Z., Verhoef, A., Verhoef, W., Batelaan, O., & Tol, C. v. d. (2011). Integration of soil moisture in SEBS for improving evapotranspiration estimation under water stress condition. *Remote Sensing of Environment (reviewing process)*.

Horst, T. W., & Weil, J. C. (1992). Footprint estimation for scalar flux measurements in the atmospheric surface layer. *Boundari-Layer Meteorology, 59*, 279-296.

Hsieh, C.-I., Katul, G., & Chi, T.-w. (2000). An approximate analytical model for footprint estimation of scalar fluxes in thermally stratified atmospheric flows. *Advances in Water Resources, 23*(7), 765-772.

ITT Visual Information Solutions. (2009). Atmospheric Correction Module: QUAC and FLAASH User's Guide ITT Visual Information Solutions,.

Kite, G. W., & Pietroniro, A. (1996). Remote sensing applications in hydrological modelling. *Hydrological Sciences Journal, 41*(4), 563-591. doi: 10.1080/02626669609491526

Lhomme, J.-P. (1997). Towards a rational definition of potential evaporation. *Hydrology and Earth System Sciences I (2)*, 257-264.

Lubczynski, M. W. (2011). *Groundwater Evapotranspiration – Underestimated Role of Tree Transpiration and Bare Soil Evaporation in Groundwater Balances of Dry Lands* (Vol. 3): Springer Netherlands.

Lubczynski, M. W., & Gurwin, J. (2005). Integration of various data sources for transient groundwater modeling with spatio-temporally variable fluxes--Sardon study case, Spain. *Journal of Hydrology, 306*(1-4), 71-96.

Matthew, M. W., Adler-Golden, S. M., Berk, A., Richtsmeier, S. C., Levine, R. Y., Bernstein, L. S., Acharya, P. K., Anderson, G. P., Felde, G. W., Hoke, M. P., Ratkowski, A., Burke, H.-H., Kaiser, R. D., & Miller, D. P. (2000). Status of Atmospheric Correction Using MODTRAN4-based Algorithm. *SPIE Proceedings, Algorithms for Multispectral, Hyperspectral, and Ultraspectral Imagery VI., 4049*, 199-207.

Peel, M. C., Finlayson, B. L., & McMahon, T. A. (2007). Updated world map of the Köppen-Geiger climate classification. *Hydrol. Earth Syst. Sci., 11*(5), 1633-1644. doi: 10.5194/hess-11-1633-2007

Purba, G., & Anderson, D. (2005). *A Brief Practical Guide to : Eddy Covariance Flux Measurements*. Nebraska, USA: LI-COR Biosciences.

Richards, L. A. (1931). Capillary conduction of liquids through porous mediums. *Journal of Applied Physics, 1*(5), 318-333.

Rwasoka, D. T. (2010). *Evapotranspiration in water limited environments : up - scaling from crown canopy to the eddy flux footprint.* University of Twente Faculty of Geo-Information and Earth Observation (MSc Thesis), Enschede.

Schaap, M. G., Leij, F. J., & van Genuchten, M. T. (2001). rosetta: a computer program for estimating soil hydraulic parameters with hierarchical pedotransfer functions. *Journal of Hydrology, 251*(3–4), 163-176.

Schuurmans, J. M., Troch, P. A., Veldhuizen, A. A., Bastiaanssen, W. G. M., & Bierkens, M. F. P. (2003). Assimilation of remotely sensed latent heat flux in a distributed hydrological model. *Advances in Water Resources, 26*(2), 151-159.

Shelton, M. L. (2008). *Hydroclimatology: perspectives and applications*. GB: Cambridge University Press.

Shunlin, L. (2001). Narrowband to broadband conversions of land surface albedo I: Algorithms. *Remote Sensing of Environment, 76*(2), 213-238.

Šimůnek, J., Šejna, M., Saito, M., Sakai, M., & van Genuchten, M. T. (2009). The HYDRUS-1D Software Package for Simulating the One-Dimensional Movement of Water, Heat, and Multiple Solutes in Variably-Saturated Media. *Version 4.08*(Department of Environmental Sciences University of California Riverside Riverside, California).

Soil Survey Division Staff. (1993). http://soils.usda.gov/technical/classification/ Retrieved January, 16, 2012

Su, Z. (2002). The surface energy balance system (SEBS) for estimation of turbulent heat fluxes. *Hydrology and Earth System Sciences. 6 (2002), 1: 85-99. - ISSN 1027-5606*.

Sumner, D. M., & Jacobs, J. M. (2005). Utility of Penman–Monteith, Priestley–Taylor, reference evapotranspiration, and pan evaporation methods to estimate pasture evapotranspiration. *Journal of Hydrology, 308*(1–4), 81-104.

Valor, E., & Caselles, V. (1996). Mapping land surface emissivity from NDVI: Application to European, African, and South American areas. *Remote Sensing of Environment, 57*(3), 167-184.

van der Kwast, J., Timmermans, W., Gieske, A., Su, Z., Olioso, A., Jia, L., Elbers, J. A., Karssenberg, D., & Jong, S. d. (2009). Evaluation of the Surface Energy Balance System (SEBS) applied to ASTER imagery with flux-measurements at the SPARC 2004 site (Barrac, Spain). *Hydrology and Earth System Sciences Discussions, 6*(1), 1165-1196.

Van Genuchten, M. T. (1980). A closed-form equation for predicting the hydraulic conductivity of unsaturated soils. *Soil Science Society of America, 44 No. 5*.

Vesala, T., Kljun, N., Rannik, Ü., Rinne, J., Sogachev, A., Markkanen, T., Sabelfeld, K., Foken, T., & Leclerc, M. Y. (2008). Flux and concentration footprint modelling: State of the art. *Environmental Pollution, 152*(3), 653-666.

Winsemius, H. C., Savenije, H. H. G., & Bastiaanssen, W. G. M. (2008). Constraining model parameters on remotely sensed evaporation: justification for distribution in ungauged basins? *Hydrology and Earth System Sciences Discussions, 5*(4), 2293-2318.

Worku, M. A. (2000). *Evaluation and assessment of temporal and spatial variability of actual evapotranspiration using remote sensing and GIS intergrated techniques.* University of Twente Faculty of Geo-Information and Earth Observation (Unpublished MSc Thesis), Enschede.

APPENDICES

Appendix - 1 Particle size analysis

No	Sample ID	Depth [cm]	Coordinate [UTM]		Soil texture [%]		
			X	Y	Sand	Silt	Clay
1	TRAB-02A_1	5	740090	4555322	47.065	35.732	17.203
2	TRAB-02B_1	5	740087	4555329	86.663	6.977	6.359
3	TRAB-02B_2	50	740087	4555329	91.741	5.242	3.017
4	TRAB-02C_1	1	740077	4555370	85.863	9.416	4.721
5	TRAB-03_1	10	740727	4555414	88.114	7.737	4.149
6	TRAB-04_1	10	740315	4555593	86.307	9.035	4.658
7	TRAB-05_1	10	740518	4555087	86.129	9.392	4.480
8	TRAB-06_1	10	740379	4554926	57.012	28.938	14.050
9	TRAB-06_2	50	740379	4554926	63.191	24.290	12.519
10	TRAB-06_3	100	740379	4554926	81.283	12.669	6.048
11	TRAB-06_4	150	740379	4554926	87.261	8.986	3.753
12	TRAB-06_5	200	740379	4554926	89.036	7.657	3.307
13	TRAB-06_6	230	740379	4554926	85.729	9.856	4.415
14	TRAB-07_1	20	739706	4555394	80.821	14.007	5.172
15	TRAB-08A_1	10	739796	4555703	86.035	9.786	4.179
16	TRAB-09A_1	10	739661	4555981	79.762	12.251	7.987
17	TRAB-09A_2	50	739661	4555981	69.908	18.092	12.000
18	TRAB-09A_3	100	739661	4555981	80.316	11.434	8.251
19	TRAB-09B_1	50	739670	4555992	76.958	12.801	10.241
20	TRAB-09B_2	100	739670	4555992	83.986	11.320	4.694
21	TRAB-10_1	10	739830	4555912	56.747	29.120	14.133
22	TRAB-12_1	50	739756	4555624	77.849	13.051	9.100
23	TRAB-12_2	97	739756	4555624	82.217	10.932	6.851
24	TRAB-13_1	10	740058	4555093	87.599	8.693	3.707
25	TRAB-14_1	10	740895	4555126	80.955	12.520	6.525
26	TRAB-15_1	10	740455	4555363	87.609	8.509	3.882
27	TRAB-17_1	10	739406	4555574	82.416	12.465	5.119
28	TRAB-19_1	10	739397	4555795	85.345	10.656	3.999
29	TRAB-21_1	10	739934	4555741	84.385	10.785	4.830
30	TS-02_1	20	739489	4555884	76.378	16.429	7.194
31	TS-02_2	50	739489	4555884	80.991	12.917	6.092
32	TS-02_3	90	739489	4555884	85.863	10.752	3.385
33	TS-02_5	140	739489	4555884	88.516	8.099	3.385
34	TS-02_7	180	739489	4555884	83.743	10.322	5.935
35	TS-02_9	220	739489	4555884	86.898	9.011	4.091

Appendix - 2 Permeameter analyses

1. Constant head analysis

No	Sample ID	Depth [cm]	Coordinate (UTM)		Ks [m/d]
			X	Y	
1	TS 02_R1	80	739489	4555884	26.78
2	TRAB 05_R1	50	740518	4555087	46.53
3	TS 02_R2	120	739489	4555884	13.49
4	TRAB 11_R1	50	739566	4555791	4.24
5	TRAB 02B_R1	50	740087	4555329	13.35
6	TRAB 16_R1	50	739997	4555480	1.01

2. Falling head analysis

No	Sample ID	Depth [cm]	Coordinate (UTM)		Ks [m/d]
			X	Y	
1	TRAB 02A_R1	50	740090	4555322	0.05349
2	TRAB 10_R2	100	739830	4555912	0.033207
3	TRAB 07_R1	50	739706	4555394	0.489746
4	TRAB 01_R1	50	739411	4555873	0.242297
5	TS 02_R3	180	739489	4555884	0.208561
6	TRAB 18_R2	100	739509	4555608	0.147203
7	TRAB 10_R1	50	739830	4555912	0.022626
8	TRAB 18_R1	50	739509	4555608	0.037929
9	TRAB 16_R1	50	739997	4555480	0.222196